ELSEVIER

Contents lists available at ScienceDirect

Wave Motion

journal homepage: www.elsevier.com/locate/wamot



The electromomentum effect in piezoelectric Willis scatterers



René Pernas-Salomón ^a, Michael R. Haberman ^{b,c}, Andrew N. Norris ^d, Gal Shmuel ^{a,*}

- a Faculty of Mechanical Engineering, Israel Institute of Technology, Haifa, Israel
- ^b Walker Department of Mechanical Engineering, The University of Texas at Austin, Austin, TX 78712-1591, USA
- ^c Applied Research Laboratories, The University of Texas at Austin, Austin, TX 78758, USA
- ^d Mechanical and Aerospace Engineering, Rutgers University, Piscataway, 2 NJ 08854-8058, USA

ARTICLE INFO

Article history: Received 11 February 2021 Received in revised form 4 June 2021 Accepted 30 June 2021 Available online 7 July 2021

Keywords:
Composites
Metamaterials
Willis materials
Scattering experiments
Piezoelectricity
Dynamic homogenization

ABSTRACT

Materials with asymmetric microstructure can constitutively couple macroscopic fields from different physics. Examples include piezoelectric materials that couple mechanical and electric fields and Willis materials that anomalously couple dynamic and elastic fields, for example velocity and stress. Recently, it was shown that anomalous coupling between the elastodynamic and electric field emerges when piezoelectricity is incorporated into Willis materials. Here, we investigate one-dimensional asymmetric piezoelectric Willis elements using heuristic homogenization, long-wavelength asymptotic analysis and numerical experiments. We show that in order to describe the heterogeneous scatterer using a homogenized description that respects reciprocity and energy conservation, anomalous electromomentum moduli must be included. Our findings elucidate the origins of this electromomentum coupling and provide insight for the future design of this new class of coupled-field metamaterials.

© 2021 Published by Elsevier B.V.

1. Introduction

Metamaterials are engineered composites materials with extraordinary effective properties that offer functionalities beyond those of standard materials [1–5]. Prominent examples in elastodynamics and acoustics include metamaterials with negative mass density and negative stiffness, which are in sharp contrast with the positive moduli of their constituents [6–9]. A separate class of metamaterials, known as Willis materials, exhibit unique properties on the macroscale that their constituents do not possess, namely, moduli that couple the momentum with the strain, and the velocity with the stress [10–14]. Willis materials therefore offer additional degrees of freedom to manipulate mechanical waves similar to the way that bianisotropic materials allow greater control over electromagnetic waves [15–20].

The emergence of these non-intuitive effective moduli is the result of a homogenization scheme for elastic composites that was initially developed by Willis [21–25] to understand the elastodynamic response of heterogeneous elastic media, and revisited by many others in the context of metamaterial research [16,17,26–35]. Of relevance to this work are the conclusions of Sieck et al. [18] and Muhlestein et al. [10], who demonstrated that constitutive relations of Willis form are required to describe a physically admissible macroscopic response, i.e., one that respects the principles of causality and passivity. This necessity is analogous to the need to include bianisotropic couplings in order to obtain a physically valid macroscopic description of the dynamic behavior of electromagnetic composites [36,37].

E-mail address: meshmuel@technion.ac.il (G. Shmuel).

^{*} Corresponding author.

By generalizing the approach of Willis [24] to account for piezoelectric constituent materials, Pernas-Salomón and Shmuel [38] have found that the dynamic response of such materials is described by constitutive relations which include effective moduli that couple the velocity and momentum of the medium to the electric fields. These generalized Willis couplings are therefore referred to as electromomentum couplings. From the viewpoint of applications, the significance of this result is twofold. First, it extends the design space of elastodynamic metamaterials beyond Willis materials to include cross-coupling with the electromagnetic domain. Second, it provides a new avenue for mechanical wave manipulation using external electric sources, as we also show in the sequel.

The homogenization procedures of Willis [23,24,39], and in turn Pernas-Salomón and Shmuel [38], are based on ensemble averaging of the microscopic fields, which provides effective constitutive relations that are nonlocal in time and space. These relations become local in space when the wavelength is much larger than the microstructure, or when they are used to describe a single subwavelength element rather than a bulk, in which case they are termed the Milton-Briane-Willis equations [15,40,41]. Analysis of the effective parameters shows that the local part of the Willis coupling coefficients originates from broken inversion asymmetry [17,18]. Recent experiments that demonstrate the local contributions to the Willis coupling were carried out in these settings, i.e., using asymmetric subwavelength structures [10,13,14,42-44]. The objective of the present work is to provide an analogous evidence of local electromomentum coupling by investigating the scattering response of asymmetric piezoelectric elements embedded in elastic background material.

We consider *Gedanken* experiments where a heterogeneous piezoelectric element separates two homogeneous elastic slabs and scatters one-dimensional strain waves incident from the slabs. We calculate analytically the experimentally measurable reflection and transmission coefficients, and develop a retrieval method to extract the effective properties from these coefficients. This simplistic approach for homogenization, based on the scattering properties of a finite slab, was first developed for electromagnetic waves [45,46], and was later adapted to acoustics [47]. As pointed out by Simovski [48], this simplistic approach has limited applicability, and its extracted effective properties often differ from the effective properties that are calculated using *rigorous* homogenization approaches, based on rational field-averaging. Simovski terms the simplistic approach as *heuristic*, since while is it not optimal, in certain cases it is nevertheless useful for obtaining insightful approximations [10,13]. This is particularly true in the low frequency, long-wavelength limit, and in the sequel we restrict attention to this limit.

We apply our heuristic homogenization scheme using two different homogenized models to describe the element: one that includes the electromomentum coupling, and one that neglects it. Borrowing the terminology in Refs. [18,36], we refer to the former model as the *effective* model and to the latter model as the *equivalent* model.

We find that the properties retrieved using the effective model satisfy reciprocity and energy conservation [18,36], and are independent of the excitation setup. By contrast, properties obtained using the *equivalent* model depend on the excitation setup, and violate reciprocity and energy conservation, even in the long-wavelength, low frequency limit. This discrepancy of the *equivalent* model stems from its inability to capture the fact that the reflection of incident plane waves has a directional phase angle that *depends on the electric field*. The electromomentum coupling captures precisely this phenomenon, and the inclusion of this coupling in the homogenized model renders it physically admissible. This demonstration is analogous to the analysis of Muhlestein et al. [10] for acoustic media where the authors demonstrated, both analytically and experimentally, that scattering from an asymmetric acoustic element can be represented with physically meaningful material properties, only if the Willis coupling is included in the homogenized constitutive relations. Specifically, they employed a heuristic homogenization method when considering two different homogenized models to describe the element: with- and without the Willis modulus, and found that only the former respects passivity and reciprocity.

We derive explicit low frequency expressions for the effective properties using Taylor series, and find that they are independent of the number of unit cells in the element. Furthermore, the leading term in the expansions of the standard properties is a real constant that agrees with the expected value from static homogenization in the limiting decoupled case. By contrast, the leading term in the expansions of the Willis coupling and the electromomentum coupling is a pure imaginary linear function of the frequency. These observations are in agreement with the observations from the long-wavelength limit of the rigorous homogenization method [38], and thereby support the validity of the heuristic homogenization method in this limit. The expansions further show that the couplings depend on the order of the composition, and that certain compositions exhibit zero Willis coupling and finite electromomentum coupling. Interestingly, we find that the design rule for such compositions, obtained using the heuristic homogenization, also holds for infinite periodic laminates whose effective properties are obtained using the rigorous homogenization. The directional phase angle of elements with zero Willis coupling and nonzero electromomentum coupling vanishes in the short circuit configuration and appears in open circuit conditions, a feature that can be harnessed to control the directional phase change by the opening and shortening of the circuit.

The analysis is presented as follows. First, we provide a short summary of the relevant governing equations in Section 2. Section 3 presents a simple analysis of plane waves in piezoelectric media with and without the electromomentum coupling, through which we highlight its effect on the characteristic elastic impedance and phase velocity. The conceptual experiments that demonstrate this effect are described in Section 4, together with the calculations of the resultant scattering and retrieved properties of the two models. Section 5 provides the low frequency expansions of the effective properties. Numerical examples are then presented in Section 6, and the paper concludes with a summary of the work and final remarks in Section 7.

2. Field equations and constitutive relations

Pernas-Salomón and Shmuel [38] developed a comprehensive dynamic homogenization theory for piezoelectric composites. Here we review the equations relevant to the current work in the local, one-dimensional, source-free settings. In the absence of body forces and free charge, a one-dimensional piezoelectric inhomogeneous medium satisfies the balance equations

$$\sigma_{,x} - p_{,t} = 0, \quad D_{,x} = 0,$$
 (1)

for the stress σ , momentum density p, and electric displacement field D, where x is the spatial coordinate. Faraday's equation for the electric field E is satisfied by setting $E = -\phi_{,x}$, where ϕ is the electric potential. At each point, the fields of Eq. (1) are related to E (or $\phi_{,x}$) and the derivatives of the axial displacement u through the constitutive equations [50]

$$\begin{pmatrix} \sigma \\ D \\ p \end{pmatrix} = \begin{pmatrix} C & B & 0 \\ B & -A & 0 \\ 0 & 0 & \rho \end{pmatrix} \begin{pmatrix} u_{,x} \\ \phi_{,x} \\ u_{,t} \end{pmatrix}, \tag{2}$$

where ρ , A, B, and C, are the mass density, and dielectric, piezoelectric, and elastic moduli, respectively, which vary in space since the medium is inhomogeneous. We clarify that attention is restricted to a reciprocal and lossless medium, such that the matrix in Eq. (2) is real and symmetric, and recall that this matrix is independent of the boundary conditions, for any homogeneous specimen that is large enough relatively to its microstructure [52]. This form of the constitutive relations is referred to as the stress-charge form, where A and C are measured under the conditions of constant strain and electric field, respectively.

With the objective of replacing the inhomogeneous medium by a homogeneous one that macroscopically behaves the same (in some appropriate sense³), Pernas-Salomón and Shmuel [38] obtained the following constitutive equations for the effective fields

$$\begin{pmatrix} \sigma \\ D \\ p \end{pmatrix} = \begin{pmatrix} \tilde{C} & \tilde{B} & \tilde{S} \\ \tilde{B} & -\tilde{A} & \tilde{W} \\ \tilde{S} & \tilde{W} & \tilde{\rho} \end{pmatrix} \begin{pmatrix} u_{,x} \\ \phi_{,x} \\ u_{,t} \end{pmatrix}, \tag{3}$$

where we have used the same notation for the effective fields and the microscopic fields, while the effective properties are distinguished by overhead tilde. Notably \tilde{S} and \tilde{W} are the emergent Willis and electromomentum coupling moduli, respectively, which appear only in the macroscopic description. We recall that Eq. (3) is the reduced form of the general relations found in Ref. [38], when considering one-dimensional media free of sources, in the long-wavelength limit. We note that the homogenization process that lead to Eq. (3) uses ensemble averaging to define the effective fields [24,25]; in the long-wavelength limit of a periodic medium, this averaging can be approximated by volume averaging. Using simple conceptual experiments, we will demonstrate that one must account for \tilde{W} in order to obtain a physically admissible effective description of piezoelectric scatterers under dynamic loading scenarios. Since the constituents of the heterogeneous medium are conservative and reciprocal, such description should also respect energy conservation and reciprocity, and also be independent of the boundary conditions.

3. Plane wave analysis and the main idea

Before we begin with the analysis of the scattering experiments, it is instructive to analyze one-dimensional plane waves in piezoelectric Willis media, through which we can highlight the role of the cross-couplings on the elastic impedance and phase velocity. To this end, we consider a homogenized medium that is governed by Eq. (3), and examine the equation of motion after we substitute the constitutive relations for σ and p. By doing so, we obtain

$$\tilde{C}u_{,xx} + \tilde{B}\phi_{,xx} - \tilde{W}\phi_{,xt} - \tilde{\rho}u_{,tt} = 0. \tag{4}$$

Note that $\tilde{S}u_{,tx}$ and $\tilde{S}u_{,xt}$ cancel out, in agreement with the observations of Muhlestein et al. [53] for the case when the Willis tensor is aligned with the direction of propagation.⁵ As is the case for standard piezoelectric media, further derivations depend on the form of the electric fields. We distinguish between the two cases: (i) short circuit for which E=0, and (ii) open circuit for which D=0. The piezoelectric analysis here extends that of Refs. [10,18,53] for purely acoustic Willis materials, and is related to the analysis by Kutsenko et al. [54] on the Bloch impedance of periodic piezoelectric media.

¹ For complete details on the theory in the general settings, see Refs. [38,49].

The dielectric and piezoelectric moduli are often denoted in the literature by ε and e instead of the notation A and B used here [50,51].

³ See Refs. [24,25,29] for details.

⁴ In periodic media, the fields have the form of a periodic function times a Bloch envelope, and then ensemble averaging is equal to averaging of the periodic part, while keeping the Bloch envelope [3,24]. Since the envelope is unity in the long-wavelength limit, in this case the two definitions of volume- and ensemble averaging coincide.

⁵ The contribution of the Willis coupling to the equations is retained in any other case where its polarization is not parallel or anti-parallel to the propagation direction [Eq. (2.8) therein].

3.1. Plane waves in short circuit configuration

The condition $E=0\equiv -\phi_{,x}$ simplifies Eq. (4) to the standard one-dimensional wave equation for an elastic medium with plane wave modulus \tilde{C} and density $\tilde{\rho}$, namely,

$$\tilde{C}u_{xx} - \tilde{\rho}u_{tt} = 0, \tag{5}$$

which is satisfied by plane wave solutions of the form $u(x,t)=Ue^{i\left(\pm \tilde{k}_{\rm E}x-\omega t\right)}$. This defines the phase velocity $\tilde{v}_{\rm E}^2:=\tilde{C}/\tilde{\rho}$ and the wavenumber $\tilde{k}_{\rm E}=\omega/\tilde{v}_{\rm E}$ in the absence of electric field. In terms of these quantities, we write the characteristic elastic impedance $Z=\sigma/u_{,t}$ in a short circuit configuration. It immediately follows from the substitution of the plane wave form into the constitutive equation for σ that $Z^\pm=\pm \tilde{Z}_{\rm E}+\tilde{S}$, where $\tilde{Z}_{\rm E}^2:=\tilde{\rho}\tilde{C}$, and the sign of the superscript for Z designates the wave direction. The implication is that when \tilde{S} exists, the impedance is asymmetric with respect to the propagation direction. This motivates us to follow Muhlestein et al. [10,53] and define the asymmetry factor in the absence of electric field, $\chi_{\rm E}=\tilde{S}/\tilde{Z}_{\rm E}$, in order to rewrite the impedance as

$$Z^{\pm} = (\pm 1 + \gamma_{\rm F})\tilde{Z}_{\rm F}.\tag{6}$$

Eq. (6) shows that the asymmetry factor χ_E in the absence of an E-field is the same as the asymmetry factor in Willis media without the electromomentum coupling. It has been established that the local Willis coupling of a reciprocal and passive medium is purely imaginary, and its leading term in a low frequency expansion is linear [17,30,55]. Accordingly, we can relate the asymmetry of Z to a purely real coupling coefficient \hat{S} through the relation $\hat{S} = i\omega \hat{S}$, that is asymptotically tractable, in terms of which we rewrite the impedance as [10]

$$Z^{\pm} = \pm \tilde{Z}_{\rm F} + i\omega \hat{S}. \tag{7}$$

Eq. (7) highlights the fact that the characteristic elastic impedance is complex and changes phase angle with direction in media with local Willis coupling. Muhlestein et al. [10] linked this impedance to the scattering behavior of an acoustic asymmetric element, and related its imaginary part to the asymmetry in the reflection coefficients when plane waves are incident from opposing directions. This asymmetric response led to their observation that one must include Willis coupling in the dynamic effective properties to obtain a physically valid effective description of the asymmetric element, since \tilde{Z}_E must be real and direction independent in order for \tilde{C} and $\tilde{\rho}$ to satisfy reciprocity and energy conservation. The remaining insights needed to understand the electromomentum coupling are obtained from the comparison with the open circuit configuration, D=0, considered next.

3.2. Plane waves in open circuit configuration

It follows from Gauss' law [Eq. $(1)_2$] that the electric displacement field is zero in the absence of free charge when the electrical components are in open circuit boundary conditions. We can then use the derivatives of Eq. $(1)_2$ and the constitutive relation for D to obtain expressions for $\phi_{,xx}$, and $\phi_{,xt}$, in order to rewrite the equation of motion (4) as

$$\left(\tilde{C} + \frac{\tilde{B}^2}{\tilde{A}}\right) u_{,xx} - \left(\tilde{\rho} + \frac{\tilde{W}^2}{\tilde{A}}\right) u_{,tt} = 0.$$
(8)

Solutions to Eq. (8) are plane waves of the form $u(x,t) = Ue^{i\left(\pm \bar{k}_D x - \omega t\right)}$ with the wavenumber $\tilde{k}_D := \omega/\tilde{v}_D$ and the phase velocity $\tilde{v}_D^2 := \tilde{C}_D/\tilde{\rho}_D$, where $\tilde{C}_D := \tilde{C} + \tilde{B}^2/\tilde{A}$ and $\tilde{\rho}_D := \tilde{\rho} + \tilde{W}^2/\tilde{A}$. This simple analysis reveals an appealing analogy between the piezoelectric effect and the electromomentum effect: the latter alters the apparent mass density in the same way that the former stiffens the apparent elastic modulus [50]. Therefore, evidence for \tilde{W} can be found in a dynamic open circuit experiment that will prove that the effective phase velocity is given by $\tilde{C}_D/\tilde{\rho}_D$, not $\tilde{C}_D/\tilde{\rho}$. More insights are obtained from the analysis of the characteristic impedance and asymmetry factor. To this end, we substitute the above form for u into the constitutive equation for σ , eliminate $\phi_{,x}$ using the constitutive equation for D=0, and obtain

$$\sigma = i\tilde{k}_{\rm D}\tilde{C}u + i\tilde{k}_{\rm D}\frac{\tilde{B}^2}{\tilde{A}}u - i\omega\frac{\tilde{W}\tilde{B}}{\tilde{A}}u - i\omega\tilde{S}u. \tag{9}$$

Using the definition of \tilde{k}_D we find that the characteristic plane wave impedance in open circuit is

$$Z^{\pm} := \frac{\sigma}{-i\omega u} = (\pm 1 + \chi_{D})\tilde{Z}_{D}, \quad \tilde{Z}_{D}^{2} := \tilde{\rho}_{D}\tilde{C}_{D}, \quad \chi_{D} := \frac{1}{Z_{D}} \left(\tilde{S} + \frac{\tilde{B}}{\tilde{A}} \tilde{W} \right), \tag{10}$$

⁶ This actually motivates a different form for the constitutive relations, in which the stress depends on the acceleration and the momentum depends on the strain rate, see Refs. [17,18,40,49].

where \tilde{Z}_D must be real for the constitutive properties to respect reciprocity and energy conservation. We again observe that the characteristic impedance is asymmetric in the propagation direction, however the asymmetry factor for the open circuit condition, χ_D , depends on both the conventional Willis modulus and the electromomentum modulus \tilde{W} . Previous works have shown that \tilde{W} —like \tilde{S} —is purely imaginary in reciprocal and conservative local media, and its leading term in a low frequency expansion is a linear function of frequency [38,49]. Therefore, we can relate the asymmetry in Z with a purely real coupling coefficient that is asymptotically tractable, say \hat{W} , through the relation $\tilde{W}=i\omega\hat{W}$, in terms of which we rewrite the impedance as

$$Z^{\pm} = \pm \tilde{Z}_{D} + i\omega \left(\hat{S} + \frac{\tilde{B}}{\tilde{A}} \hat{W} \right). \tag{11}$$

Eq. (11) indicates that the electromomentum coefficient alters the directional dependence by altering the phase angle in addition to the \hat{S} contribution. This suggests a simple test for the existence of \tilde{W} : Examine the directional phase change of waves that are reflected from an asymmetric piezoelectric element in scattering experiments, both in short and open circuit configurations; if they do not match, it will provide evidence that \tilde{W} is non-zero and must be considered in order to determine physically meaningful effective properties of the medium. This is precisely what we demonstrate in the sections that follow by extending the scheme of Muhlestein et al. [10] to piezoelectric media.

4. Scattering from a piezoelectric Willis element

Consider a piezoelectric stack connecting two semi-infinite slabs made of an elastic isotropic material with plane wave modulus C_0 and density ρ_0 . The piezoelectric stack comprises three layers, 1, 2 and 3, of lengths l_1 , l_2 and l_3 , respectively, as shown in Fig. 1. Thin electrodes are located at the interfaces between the stack and the elastic slabs. Having set up the Gedanken experimental apparatus, we conduct a scattering analysis, from which we analytically determine the transmission and reflection coefficients of the piezoelectric stack. We will use these coefficients in an inverse program to determine the effective properties of a fictitious homogenized medium that reproduces the same scattering that the heterogeneous stack generates [10,47,56]. The retrieved effective properties of the homogenized medium depend on the model chosen for its constitutive relations. It is important to note that while the analysis that follows considers a single, heterogeneous scatterer, which can also be understood as a unit cell from the perspective of polarizability [11,14,18,37,56], the approach employed here is representative of experimental methods used to characterize material properties and can be extended to consider the response of many unit cells [10]. In this section, we describe a scheme to retrieve the effective properties based on two homogenized models: one that includes the electromomentum coupling [Eq. (3)], and one equivalent model that neglects it. We will show that while the latter model delivers (by construction) the same scattering coefficients as our effective model (hence the term equivalent), the resulting properties violate reciprocity and energy conservation and therefore lack physical meaning. Further, the properties retrieved using the equivalent model depend on the excitation setup, even in the low frequency limit.

4.1. Retrieved properties from short circuit conditions

Consider a setup where the two electrodes at the ends of the piezoelectric stack are connected in a short circuit configuration (switch is closed in Fig. 1), such that the average (or effective) electric field is null. Two experiments are considered in this configuration: in experiment L (resp. R), the stack is excited by a time-harmonic longitudinal wave that is incoming from the left slab (resp. right). The incident wave is partly reflected at the interface with the stack and partly transmitted to the opposite slab. We assume a time dependency $e^{-i\omega t}$ and write the resultant displacement field in the elastic slabs as

$$u(x,t) = \begin{cases} \left(c_{L}^{+}e^{ik_{0}x} + c_{L}^{-}e^{-ik_{0}x}\right)e^{-i\omega t}, & x \leq x_{0}, \\ \left(c_{R}^{+}e^{ik_{0}x} + c_{R}^{-}e^{-ik_{0}x}\right)e^{-i\omega t}, & x \geq x_{3}, \end{cases}$$
 $k_{0} = \omega\sqrt{\frac{\rho_{0}}{C_{0}}}$ (12)

where c_L^+ (resp. c_R^-) is the prescribed amplitude of the incident wave in experiment L (resp. R), and c_R^- (resp. c_L^+) is zero. These experimentally measurable coefficients can be calculated analytically by introducing the state vector $\mathbf{h}(\mathbf{x})^8$ that is continuous in \mathbf{x} ,

$$h(x) = (u, \phi, \sigma, D)^{\mathsf{T}}. \tag{13}$$

⁷ This motivates a different form for the constitutive relations, in which the electric displacement field depends on the acceleration and the momentum depends on the time rate of the electric field, see Ref. [49].

⁸ Henceforth, with an abuse of notation, we omit the dependency on t, and recall that it is always in the form $e^{-i\omega t}$.

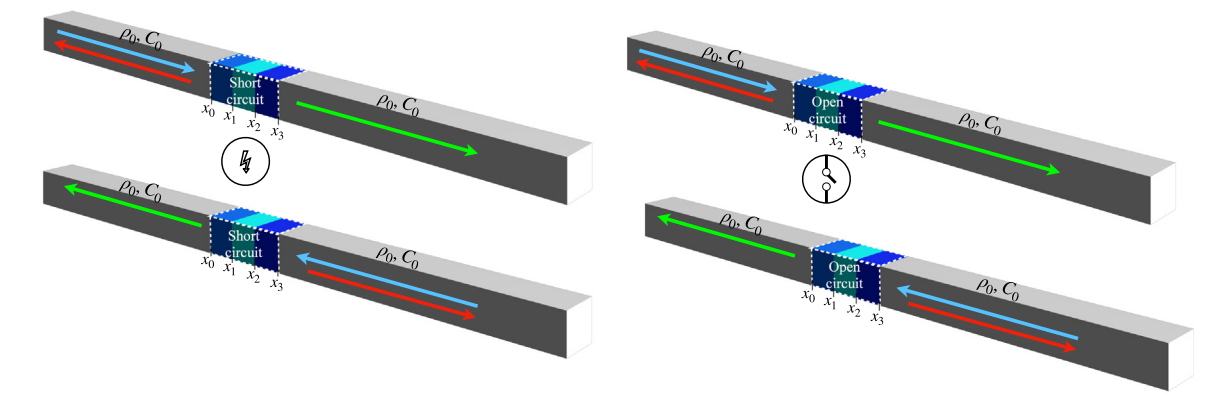


Fig. 1. Schematics of the *Gedanken* experiments on a piezoelectric element covered by electrodes at x_0 and x_3 . The element is made of three layers which connect two semi-infinite elastic slabs made of an isotropic material with plane wave modulus C_0 and density ρ_0 . When the switch is closed (figures in the left column) and open (figures in the right column), the setup corresponds to short- and open circuit electric boundary conditions, respectively. For each setup, we analyze an experiment where the incident waves are incoming from the left waveguide (figures at the top row), and an experiment where the incident waves are incoming from the right waveguide (figures at the bottom row). Incident, transmitted and reflected waves are denoted by light blue, green and red arrows. The phase of the reflected waves depends on the direction of the incoming waves and the electric circuit conditions. This dependency is captured by the electromomentum coupling. (For interpretation of the references to color in this figure legend, the reader is referred to the web version of this article.)

The values of h(x) at the ends x_{n-1} and x_n of the nth piezoelectric layer are related via [54]

$$h(x_n) = \mathsf{T}_n^{\text{em}} \, h(x_{n-1}), \quad \mathsf{T}_n^{\text{em}} = \begin{pmatrix} \cos k_{Dn} l_n & 0 & \sin k_{Dn} l_n / \omega Z_{Dn} & \frac{B_n}{A_n} \sin k_{Dn} l_n / \omega Z_{Dn} \\ \frac{B_n}{A_n} \left(\cos k_{Dn} l_n - 1\right) & 1 & \frac{B_n}{A_n} \sin k_{Dn} l_n / \omega Z_{Dn} & \left(\frac{B_n}{A_n}\right)^2 \sin k_{Dn} l_n / \omega Z_{Dn} - \frac{l_n}{A_n} \\ -\omega Z_{Dn} \sin k_{Dn} l_n & 0 & \cos k_{Dn} l_n & \frac{B_n}{A_n} \left(\cos k_{Dn} l_n - 1\right) \\ 0 & 0 & 0 & 1 \end{pmatrix}, \tag{14}$$

where $k_{Dn} = \omega \sqrt{\rho_n/C_{Dn}}$, $Z_{Dn} = \sqrt{\rho_n C_{Dn}}$ and $C_{Dn} = (C_n + B_n^2/A_n)$. Continuity of h(x) implies that

$$h(x_3) = T^L h(x_0), \quad T^L = T_3^{em} T_2^{em} T_1^{em},$$
 (15)

in experiment L, while in experiment R, the composition order of T_n^{em} is reversed. We focus first on experiment L. In this case, it follows from Eq. (15) that

$$\phi(x_3) - \phi(x_0) = \mathsf{T}_{21}^{\mathsf{L}} u(x_0) + \mathsf{T}_{23}^{\mathsf{L}} \sigma(x_0) + \mathsf{T}_{24}^{\mathsf{L}} D, \tag{16}$$

where $\mathsf{T}^{\mathsf{L}}_{ij}$ is the ij-component of the matrix T^{L} , and we have used the fact that electric displacement is constant inside the stack. Since the electrodes are in short circuit such that the potential difference is zero, i.e., $\phi(x_3) - \phi(x_0) = 0$, then Eq. (16) together with Eq. (15) implies

$$\begin{pmatrix} u(x_3) \\ \sigma(x_3) \end{pmatrix} = \mathsf{T}^{\mathsf{s}}(x_3, x_0) \begin{pmatrix} u(x_0) \\ \sigma(x_0) \end{pmatrix}, \quad \mathsf{T}^{\mathsf{s}} = \begin{pmatrix} \mathsf{T}^{\mathsf{L}}_{11} - \frac{\mathsf{T}^{\mathsf{L}}_{14}}{\mathsf{T}^{\mathsf{L}}_{24}} \mathsf{T}^{\mathsf{L}}_{21} & \mathsf{T}^{\mathsf{L}}_{13} - \frac{\mathsf{T}^{\mathsf{L}}_{14}}{\mathsf{T}^{\mathsf{L}}_{24}} \mathsf{T}^{\mathsf{L}}_{23} \\ \mathsf{T}^{\mathsf{L}}_{31} - \frac{\mathsf{T}^{\mathsf{L}}_{34}}{\mathsf{T}^{\mathsf{L}}_{24}} \mathsf{T}^{\mathsf{L}}_{21} & \mathsf{T}^{\mathsf{L}}_{33} - \frac{\mathsf{T}^{\mathsf{L}}_{34}}{\mathsf{T}^{\mathsf{L}}_{24}} \mathsf{T}^{\mathsf{L}}_{23} \end{pmatrix}. \tag{17}$$

Eq. (17) relates the displacement and stress at the two ends of the stack, and hence the amplitudes of the incoming and outgoing waves. By applying the continuity conditions for the displacement and stress fields at x_0 and x_3 and using Eqs. (12) and (17), we relate the amplitudes of the waves through the following coefficients transfer matrix

$$\begin{pmatrix} c_{R}^{+} \\ c_{R}^{-} \end{pmatrix} = K^{s}(R, L) \begin{pmatrix} c_{L}^{+} \\ c_{L}^{-} \end{pmatrix}, \tag{18}$$

where

$$K^{s}(R, L) = Q_{0}(x_{3})^{-1}T^{s}(x_{3}, x_{0})Q_{0}(x_{0}), \quad Q_{0}(x) = \begin{pmatrix} e^{ik_{0}x} & e^{-ik_{0}x} \\ iC_{0}k_{0}e^{ik_{0}x} & -iC_{0}k_{0}e^{-ik_{0}x} \end{pmatrix}.$$

$$(19)$$

Eq. (18) returns the output of experiment L when $c_R^-=0$ with the reflection and transmission amplitudes $r_L=c_L^-/c_L^+$ and $t_L=c_R^+/c_L^+$, respectively. Similarly, Eq. (18) returns the output of experiment R using $c_L^+=0$ with the reflection

and transmission amplitudes $r_R = c_R^+/c_R^-$ and $t_R = c_L^-/c_R^-$, respectively. The matrix K^s can be expressed in terms of these amplitudes [57], namely,

$$\mathsf{K}^{\mathsf{s}}(\mathsf{R},\mathsf{L}) = \begin{pmatrix} t_{\mathsf{L}} - r_{\mathsf{R}} t_{\mathsf{R}}^{-1} r_{\mathsf{L}} & r_{\mathsf{R}} t_{\mathsf{R}}^{-1} \\ -r_{\mathsf{L}} t_{\mathsf{R}}^{-1} & t_{\mathsf{R}}^{-1} \end{pmatrix}. \tag{20}$$

Eqs. (17)–(20) together imply the L-experimental results

$$t_{\rm L} = 2e^{-ik_0l} \left(\mathsf{T}_{22}^{\rm s} + \mathsf{T}_{11}^{\rm s} - i\omega Z_0 \mathsf{T}_{12}^{\rm s} - (i\omega Z_0)^{-1} \mathsf{T}_{21}^{\rm s} \right)^{-1},\tag{21a}$$

$$r_{L} = \left(\mathsf{T}_{22}^{\mathsf{s}} - \mathsf{T}_{11}^{\mathsf{s}} - i\omega Z_{0}\mathsf{T}_{12}^{\mathsf{s}} + (i\omega Z_{0})^{-1}\mathsf{T}_{21}^{\mathsf{s}}\right) \frac{t_{L}}{2}. \tag{21b}$$

The analysis for experiment R mirrors the above procedure, showing that r_R and t_R equal, respectively, the right hand sides of Eqs. (21a) and (21b), after replacing $T_{ij}^s(T^L)$ by $T_{ij}^s(T^R)$. Notably, we find $t_L \equiv t_R$, as expected for a reciprocal medium, while the phase of r_L may differ from the phase of r_R . This difference depends on the spatial asymmetry of the stack, and is a manifestation of the directional dependency of the effective characteristic impedance, as discussed in Section 3.1.

The objective now is to determine the properties of a fictitious homogeneous medium that exhibits the same scattering coefficients as the stack, i.e., will reproduce the same $K^s(R, L)$ —under the same boundary conditions. As per this short circuit configuration, the electric field in the fictitious homogeneous medium should vanish, like the average electric field in the stack. The constitutive relations for σ and p of both the effective and equivalent models reduce to

$$\sigma = \tilde{C}u_{,x} - i\omega\tilde{S}u,\tag{22a}$$

$$p = \tilde{S}^{\dagger} u_{,x} - i\omega \tilde{\rho} u. \tag{22b}$$

(Later on, we will use superscript eq to distinguish the retrieved properties of the *equivalent* model that neglects \tilde{W} from the retrieved properties of the effective that includes \tilde{W}). In this case, the constitutive equations for σ and p [Eq. 22a] involve only the effective mechanical properties and thus reduce to the Willis form, in agreement with the analysis provided in Section 3.1.

We note that unlike in Eq. (3), Eq. (22b) does not assume a priori that the conditions imposed by reciprocity are satisfied [17,49], which would imply that the coupling between σ and $u_{,t}$ is equal to the coupling between p and $u_{,x}$. To maintain the additional generality, we denote by \tilde{S}^{\dagger} the coefficient that couples p with $u_{,x}$, and show by analysis that $\tilde{S} = \tilde{S}^{\dagger}$. Before we proceed to determine \tilde{C} , $\tilde{\rho}$, \tilde{S} and \tilde{S}^{\dagger} , we emphasize that the remaining constitutive equation for the electric displacement field depends on the form of the chosen model, i.e., whether or not it accounts for the electromomentum coupling. This will be addressed in Section 4.2.

To determine the properties \tilde{C} , $\tilde{\rho}$, \tilde{S} and \tilde{S}^{\dagger} of a fictitious homogenized medium with the same scattering response as the stack, we relate the displacement and stress fields at the ends of the homogenized medium via (Appendix A)

$$\begin{pmatrix} u(x_3) \\ \sigma(x_3) \end{pmatrix} = \mathsf{T}^{\mathsf{m}}(x_3, x_0) \begin{pmatrix} u(x_0) \\ \sigma(x_0) \end{pmatrix},\tag{23}$$

where $T^{m}(x_3, x_0) = e^{lM}$ is the transfer matrix of the homogenized medium, defined by

$$\mathsf{M} = \begin{pmatrix} i\omega\tilde{S}\tilde{C}^{-1} & \tilde{C}^{-1} \\ \omega^2\tilde{S}\tilde{S}^{\dagger}\tilde{C}^{-1} - \omega^2\tilde{\rho} & -i\omega\tilde{S}^{\dagger}\tilde{C}^{-1} \end{pmatrix}. \tag{24}$$

We enforce the homogenized medium to reproduce the same scattering properties, i.e., the same K^s . This implies that the variables in Eq. (24) are determined from [see Eqs. (19)–(20)]

$$Q_0^{-1}(x_3)T^{m}Q_0(x_0) = \begin{pmatrix} t_L - r_R t_R^{-1} r_L & r_R t_R^{-1} \\ -r_L t_R^{-1} & t_R^{-1} \end{pmatrix},$$
(25)

which yields equations for T^m in terms of the reflection and transmission coefficients r_L , r_R , t_L and t_R . Recalling $t_L \equiv t_R =: t$, simplifies T^m to

$$\mathsf{T}^{\rm m} = \frac{1}{2t} \left(\begin{array}{cc} \vartheta e^{ik_0 l} + e^{-ik_0 l} + r_{\rm R} - r_{\rm L} & \frac{1}{i\omega Z_0} \left[\vartheta e^{ik_0 l} - e^{-ik_0 l} - r_{\rm R} - r_{\rm L} \right] \\ i\omega Z_0 \left[\vartheta e^{ik_0 l} - e^{-ik_0 l} + r_{\rm R} + r_{\rm L} \right] & \vartheta e^{ik_0 l} + e^{-ik_0 l} - r_{\rm R} + r_{\rm L} \end{array} \right), \tag{26}$$

where $\vartheta = t^2 - r_L r_R$, and $Z_0 = \sqrt{\rho_0 C_0}$ is the characteristic impedance of the elastic slabs. By applying Sylvester's formula to the logarithm of T^m, Eq. (26) admits the following simplification [27,58,59]

$$\mathsf{M} = \frac{\psi}{l\sin\psi} \left(\mathsf{T}^{\mathsf{m}} - \frac{1}{2}\mathsf{I}\,\mathsf{tr}\mathsf{T}^{\mathsf{m}} \right), \quad \cos\psi = \frac{1}{2}\mathsf{tr}\mathsf{T}^{\mathsf{m}} = \frac{\vartheta e^{ik_0l} + e^{-ik_0l}}{2t},\tag{27}$$

where $e^{\pm i\psi}$ are the eigenvalues of T^m. We deduce from Eq. (27) that $M_{22}=-M_{11}$, and the effective elastic properties are

$$\tilde{S} = \frac{M_{11}}{i\omega M_{12}} = \frac{Z_0 (r_R - r_L)}{(t^2 - r_L r_R) e^{ik_0 l} - e^{-ik_0 l} - r_R - r_L},$$
(28a)

$$\tilde{S}^{\dagger} = -\frac{M_{22}}{i\omega M_{12}} \equiv \tilde{S},\tag{28b}$$

$$\tilde{C} = M_{12}^{-1} = \frac{2i\omega Z_0 lt \psi^{-1} \sin \psi}{(t^2 - r_L r_R) e^{ik_0 l} - e^{-ik_0 l} - r_R - r_L},$$
(28c)

$$\tilde{\rho} = \frac{\det M}{\omega^2 M_{12}} = \frac{-iZ_0 \psi}{2t\omega l \sin \psi} \left[\frac{\left(\left(t^2 - r_L r_R \right) e^{ik_0 l} - e^{-ik_0 l} \right)^2 - 4r_R r_L}{\left(t^2 - r_L r_R \right) e^{ik_0 l} - e^{-ik_0 l} - r_R - r_L} \right], \tag{28d}$$

where, as mentioned, in this setup the elastic *equivalent* properties are equal to the elastic effective properties. Eq. (28) expresses the effective properties directly in terms of the experimentally measurable scattering coefficients [which were analytically calculated using Eq. (21)]. Thus, by construction, the retrieved models deliver the same scattering response that the piezoelectric stack produces. The above experiments are consistent with the conditions that are required to evaluate the properties of a standard piezoelectric material in the stress-charge form, in the sense that the stiffness was evaluated at a prescribed (effective) electric field.

To summarize the results of our *Gedanken* experiments so far: we find frequency-dependent effective properties, even though the assumed properties of each constituent are frequency-independent. Notably, the Willis couplings \tilde{S} and \tilde{S}^{\dagger} are equal one to another and depend on the spatial asymmetry of the stack through $r_R - r_L$. If the stack has certain symmetry properties, then the reflection of incoming waves from the right is the same as from the left and the Willis couplings vanish, as we will explicitly show later using low frequency approximations for the dynamic effective properties.

4.1.1. First inconsistency in retrieving the piezoelectric coefficient when neglecting \tilde{W}

A different perspective on the retrieval process is to consider the retrieved properties as those that relate the effective fields in the piezoelectric element. In the low frequency, long-wavelength limit, the effective fields are defined as the volume average of the microscopic fields. Evaluating the volume averages over the constitutive relations for σ and p delivers equations for $\tilde{\rho}$, \tilde{C} and \tilde{S} that are consistent with Eq. (28). The third equation for D, namely,

$$\langle D \rangle = \tilde{B} \langle u_{,x} \rangle - i\omega \tilde{W} \langle u \rangle , \qquad (29)$$

is not sufficient to determine \tilde{B} and \tilde{W} . If we ignore the electromomentum effect, i.e., we assume that the effective electric displacement is independent of the effective velocity field, then this experiment is sufficient to determine the *equivalent* piezoelectric coefficient \tilde{B}^{eq} from the average fields. Specifically, an additional equation for \tilde{B}^{eq} is obtained from the requirement that the *equivalent* properties of the homogenized model deliver the same average fields that are generated in the piezoelectric stack. Thus, when \tilde{W} is neglected in Eq. (3), the *equivalent* piezoelectric coefficient is determined from the relationship

$$\langle D \rangle = \tilde{B}^{\text{eq}} \langle u_{,x} \rangle, \text{ so } \tilde{B}^{\text{eq}} = \frac{\langle D \rangle}{\langle u_{,x} \rangle},$$
 (30)

where $\langle \rangle$ denotes volume averaging over $x_0 \leq x \leq x_3$. Now, if \tilde{B}^{eq} is to satisfy energy conservation and reciprocity, in the long-wavelength limit it should be a real-valued quantity that is independent of the direction of the wave. Stating explicitly the implication of the latter condition to our analysis, it requires that $\tilde{B}_L^{\text{eq}} := \langle D \rangle_L / \langle u, x \rangle_L$ will be equal to $\tilde{B}_R^{\text{eq}} := \langle D \rangle_R / \langle u, x \rangle_R$, where we recall that subscripts L and R correspond to fields that are generated in the left $(c_L^+ = 1, c_R^- = 0)$ and right $(c_L^+ = 0, c_R^- = 1)$ experiments. However, using Eq. (16) to determine $\langle D \rangle_\alpha$ and Eq. (12) to express $\langle u, x \rangle_\alpha$ in terms of the scattering coefficients, we find that

$$\tilde{B}_{\alpha}^{\text{eq}} = \frac{l \left[T_{21}^{\alpha} + i\omega Z_0 T_{23}^{\alpha} + r_{\alpha} e^{ik_0 l} \left(T_{21}^{\alpha} - i\omega Z_0 T_{23}^{\alpha} \right) \right]}{\left(1 + (r_{\alpha} - t) e^{ik_0 l} \right) T_{24}^{\alpha}}, \quad \alpha = L, R,$$
(31)

implying that $\tilde{B}_{L}^{eq} \neq \tilde{B}_{R}^{eq}$ and moreover $\text{Im}[\tilde{B}_{\alpha}^{eq}] \neq 0$. These nonphysical artifacts are generated when neglecting the electromomentum effect and persist in the low frequency limit, as we will demonstrate in Section 6.

Before we proceed to analyze the open circuit configuration, we summarize the results from the short circuit configuration. We have calculated the reflection and transmission coefficients for incidence from both sides of the heterogeneous scatterer. In terms of these coefficients, we have estimated the effective short circuit dynamic stiffness, \tilde{C} , the short circuit dynamic density $\tilde{\rho}$, and the Willis coupling, \tilde{S} . We have demonstrated that neglecting electromomentum

⁹ Again, we recall that the use of volume averages instead of ensemble averages is valid only in the long-wavelength, low frequency regime.

coupling leads to estimates for the piezoelectric coefficient that violate reciprocity and energy conservation (if the scatterer is asymmetric).

The equations that the short circuit configuration provide do not allow the extraction of the electromomentum coefficient and the dynamic effective dielectric permittivity; these will be determined using scattering experiments on the heterogeneous scatterer in the open circuit configuration. The open circuit configuration will also demonstrate that the retrieved properties using the *equivalent* description are inconsistent as they depend on the electric boundary conditions, even in the long-wavelength limit. This observation further reinforces the necessity of including electromomentum coupling in heterogeneous piezoelectric media with subwavelength-scale asymmetry.

4.2. Retrieved properties from an open circuit experiment

Consider next the same scattering problems as in Section 4.1, only now the stack is in an open circuit configuration, i.e., the switch is open in Fig. 1. We repeat the same analysis described in Section 4.1 now accounting for D=0. The objective is to retrieve the homogenized material properties in terms of the reflection and transmission coefficients in open circuit conditions, now denoted by r_{Lo} , r_{Ro} , t_o . Accordingly, we modify Eq. (15) when considering a null D-field, and obtain [cf. Eq. (17)]

$$\begin{pmatrix} u(x_3) \\ \sigma(x_3) \end{pmatrix} = \mathsf{T}^{\mathsf{o}} \begin{pmatrix} u(x_0) \\ \sigma(x_0) \end{pmatrix}, \ \mathsf{T}^{\mathsf{o}} = \begin{pmatrix} \mathsf{T}_{11}^{\mathsf{L}} & \mathsf{T}_{13}^{\mathsf{L}} \\ \mathsf{T}_{31}^{\mathsf{L}} & \mathsf{T}_{33}^{\mathsf{L}} \end{pmatrix}. \tag{32}$$

We relate the transfer matrix T^o to the reflection and transmission coefficients according to Eqs. (19)–(21) and find that for experiment L the coefficients r_{Lo} and t_{Lo} satisfy Eqs. (21b) and (21a) when T^o replaces T^s . The analysis for experiment R mirrors the procedure described above, showing that r_{Ro} and t_{Ro} equal, respectively, to the right-hand side of Eqs. (21b) and (21a), where $T^o(T^L)$ is replaced by $T^o(T^R)$. It is clear that the scattering coefficients in this experiment are different from the coefficients in the short circuit experiment, in view of the difference between T^o and T^s . Again, we find that $t_{Lo} \equiv t_{Ro}$, as it should, while r_{Lo} and r_{Ro} differ by a phase.

As in Section 4.1, we require the properties of the fictitious homogeneous medium to exhibit the same scattering coefficients as the stack when subjected to the same electrical boundary conditions. We will develop the equations using the effective model, and recall that the equations for the *equivalent* model are obtained by setting $\tilde{W}=0$. Since we consider here an open circuit configuration, the *D*-field in the fictitious homogeneous medium is null, and hence its constitutive equation for *D* provides the relation

$$\phi_{,x} = \tilde{A}^{-1} (\tilde{B}u_{,x} - i\omega \tilde{W}u). \tag{33}$$

Subsequently, we employ this relation to replace $\phi_{,x}$ in the constitutive relations for σ and p, which now read

$$\sigma = \left(\tilde{C} + \frac{\tilde{B}^2}{\tilde{A}}\right) u_{,x} - i\omega \left(\tilde{S} + \frac{\tilde{B}}{\tilde{A}}\tilde{W}\right) u,\tag{34a}$$

$$p = \left(\tilde{S}^{\dagger} + \frac{\tilde{B}}{\tilde{A}}\tilde{W}^{\dagger}\right)u_{,x} - i\omega\left(\tilde{\rho} + \frac{\tilde{W}\tilde{W}^{\dagger}}{\tilde{A}}\right)u. \tag{34b}$$

Finally, we repeat Eqs. (23)–(25) using the transfer matrix that is based on Eq. (34), and denote its logarithm by M°. The resultant relationships for the effective dynamic properties are

$$\tilde{S} + \frac{\tilde{B}}{\tilde{A}} \tilde{W} = \frac{M_{11}^{0}}{i\omega M_{12}^{0}} = \frac{Z_{0} (r_{R0} - r_{L0})}{(t_{0}^{2} - r_{L0}r_{R0}) e^{ik_{0}l} - e^{-ik_{0}l} - r_{R0} - r_{L0}},$$
(35a)

$$\tilde{S}^{\dagger} + \frac{\tilde{B}}{\tilde{A}} \tilde{W}^{\dagger} = -\frac{M_{22}^{\circ}}{i\omega M_{12}^{\circ}} \equiv \tilde{S} + \frac{\tilde{B}}{\tilde{A}} \tilde{W}, \tag{35b}$$

$$\tilde{C} + \frac{\tilde{B}^2}{\tilde{A}} = M_{12}^{0-1} = \frac{2i\omega Z_0 l t_0 \psi_o^{-1} \sin \psi_o}{\left(t_o^2 - r_{\text{Lo}} r_{\text{Ro}}\right) e^{ik_0 l} - e^{-ik_0 l} - r_{\text{Ro}} - r_{\text{Lo}}},\tag{35c}$$

$$\tilde{\rho} + \frac{\tilde{W}\tilde{W}^{\dagger}}{\tilde{A}} = \frac{\det M^{o}}{\omega^{2}M_{12}} = \frac{-i\rho_{0}\psi_{o}}{2t_{o}k_{o}l\sin\psi_{o}} \left[\frac{\left(\left(t_{o}^{2} - r_{\text{Lo}}r_{\text{Ro}} \right)e^{ik_{o}l} - e^{-ik_{o}l} \right)^{2} - 4r_{\text{Ro}}r_{\text{Lo}}}{\left(t_{o}^{2} - r_{\text{Lo}}r_{\text{Ro}} \right)e^{ik_{o}l} - e^{-ik_{o}l} - r_{\text{Ro}} - r_{\text{Lo}}} \right], \tag{35d}$$

where

$$\cos \psi^{0} = \frac{\left(t_{o}^{2} - r_{Lo}r_{Ro}\right)e^{ik_{0}l} + e^{-ik_{0}l}}{2t_{o}}.$$
(36)

Eq. (35) explicitly illustrates the electromomentum scattering contribution to the extracted effective properties. Eq. (35a) shows that the electromomentum coupling contributes to the asymmetry in the reflection, in addition to the asymmetry

associated with the Willis coefficient, \tilde{S} . Further, Eq. (35d) shows that the presence of electromomentum coupling modifies the apparent effective dynamic mass density. These phenomena are in agreement with the analysis in Section 3.

The above analysis was based on the effective model that includes \tilde{W} . The procedure to retrieve the homogenized properties using the *equivalent* model is the same up to setting $\tilde{W}=0$. Accordingly, the *equivalent* properties \tilde{S}^{eq} , $\tilde{S}^{\dagger eq}$ and $\tilde{\rho}^{eq}$ are equal to the right-hand side of Eqs. (35a), (35b) and (35d), respectively. This results in a second inconsistency in the model that neglects the electromomentum coupling: the *equivalent* properties depend on the electrical boundary conditions, since Eqs. (28) and (35) provide different values for the foregoing properties. If we denote *equivalent* properties that are extracted from short- and open circuit conditions by subscript s and o, respectively, then $\tilde{S}^{eq}_s \neq \tilde{S}^{eq}_o$, $\tilde{S}^{eq}_s \neq \tilde{S}^{eq}_o$ and $\tilde{\rho}^{eq}_s \neq \tilde{\rho}^{eq}_o$. This type of dependency of the retrieved properties of inappropriate models on the experimental setup was noted before in Refs. [18,37].

Having pointed out the second inconsistency in the *equivalent* model which reinforces the need to include electromomentum coupling, we proceed to determine the effective electromechanical properties in the fully coupled medium. We first observe that Eq. (35b) implies

$$\tilde{W} = \tilde{W}^{\dagger}, \tag{37}$$

where we used the fact that $\tilde{S} \equiv \tilde{S}^{\dagger}$ from Eq. (28b). While there are three additional equations in Eq. (35), the remaining three coefficients $(\tilde{A}, \tilde{B} \text{ and } \tilde{W})$ cannot be determined uniquely, since they enter the equations as products. Therefore, one more independent equation is required, which is obtained from the condition on the spatial average of the constitutive equation for D (cf. Section 4.1.1):

$$0 = \tilde{B}\langle u_{,x} \rangle - \tilde{A}\langle \phi_{,x} \rangle - i\omega \tilde{W} \langle u \rangle. \tag{38}$$

[Alternatively, as the third equation it is possible to use the corresponding equation from the short circuit experiment, namely, Eq. (29). In fact, we use Eq. (29) as a consistency check for the effective properties to be independent of the experimental setup.]

Having at hand the solutions for the field variables u and ϕ , we use Eq. (38) together with Eq. (35) to obtain expressions for the rest of the effective properties. We omit these lengthy expressions here, and analyze their low frequency expansions in Section 5. Before doing so, we emphasize that there are two assumptions in the procedure described above. (i) We assume that the effective properties relate volume averages instead of ensemble averages; (ii) We assume that the retrieved quantities – which depend on the surface data – indeed characterize the effective properties. These assumptions are valid only in the low frequency, long-wavelength (i) regime [1,10]. In this regime, the effective properties that result from the process are independent of the experimental setup, i.e., independent of the electrical boundary conditions. By contrast, the equivalent properties depend on these conditions, even in the low frequency, long-wavelength limit. We have validated the consistency of the effective model by comparing the effective properties computed here with the effective properties that are calculated from another electrical setup. In this third setup, the piezoelectric element is subjected to a time harmonic voltage drop, while its boundaries are kept clamped (see analysis in Appendix B). In the next section, we provide the low frequency approximations of the effective properties using Taylor expansions. As per the discussion above, the leading terms in these expansions for the effective properties are independent of the experimental setup.

5. Low frequency approximations

5.1. Peano expansion

To derive explicit expressions in the low frequency, long-wavelength limit, it proves useful to first analyze the reflection and transmission coefficients. To this end, we use the Peano expansion [60] for the transfer matrix of the layers;

$$\mathsf{T}^{\alpha} = \mathsf{I}_{4\times4} + l\,\langle\mathsf{M}\rangle + \mathcal{O}\left(\omega^{2}\right), \quad \mathsf{M}_{n} = \begin{pmatrix} 0 & 0 & C_{\mathsf{D}n}^{-1} & \frac{B_{n}}{A_{n}C_{\mathsf{D}n}} \\ 0 & 0 & \frac{B_{n}}{A_{n}C_{\mathsf{D}n}} & -\frac{C_{n}}{A_{n}C_{\mathsf{D}n}} \\ -\rho_{n}\omega^{2} & 0 & 0 & 0 \\ 0 & 0 & 0 & 0 \end{pmatrix}, \tag{39}$$

where we recall that α denotes the direction of the incident waves, and note that the terms of order ω^2 depend on this direction. Using this expression in Eq. (21) provides the following power series expansions for the coefficients in the short circuit experiment:

$$r_{\rm R} \approx r_{\rm L} = \frac{ik_0 l}{2} \left[\rho_0^{-1} \langle \rho \rangle - C_0 \left(\langle C_{\rm D}^{-1} \rangle + \gamma \left(\frac{B}{AC_{\rm D}} \right) \right) \right] + \mathcal{O} \left(\omega^2 \right), \quad \gamma = \left\langle \frac{B}{AC_{\rm D}} \right\rangle \left\langle \frac{C}{AC_{\rm D}} \right\rangle^{-1}, \tag{40a}$$

$$r_{\rm L} - r_{\rm R} = \omega^2 \sum_{p=1}^2 \sum_{q=p+1}^3 \frac{l_p l_q}{C_{\rm Dp} C_{\rm Dq}} \left[\Delta_{qp} \left(Z_{\rm D}^2 \right) + \gamma \frac{B_p B_q}{A_p A_q} \Delta_{qp} \left(\frac{A}{B} Z_{\rm D}^2 \right) \right] + \mathcal{O} \left(\omega^3 \right), \tag{40b}$$

$$t = 1 + \frac{ik_0l}{2} \left[\rho_0^{-1} \langle \rho \rangle + C_0 \left(\langle C_D^{-1} \rangle + \gamma \left(\frac{B}{AC_D} \right) \right) - 2 \right] + \mathcal{O} \left(\omega^2 \right), \tag{40c}$$

where $\Delta_{qp}f := f_p - f_q$ is the difference between the value of f in layer p and layer q. Carrying out the same procedure for the coefficients of the open circuit experiment shows that the coefficients have the same form as in Eq. (40), only now the terms that involve products with γ do not appear. Eq. (40b) shows that the leading term in the difference between the right- and left reflection coefficients is of order ω^2 , and depends on the asymmetry in the electromechanical properties of the scatterer.

5.2. Explicit low frequency expressions

Using the expression for the transmission and reflection coefficients, we derive the Taylor expansion 10 of the effective properties [Eqs. (28), (B.10) and (B.13)] about $\omega = 0$. After some rearrangement of terms we obtain

$$\tilde{\rho} = \langle \rho \rangle + \mathcal{O}\left(\omega^2\right),\tag{41a}$$

$$\tilde{C} = \left[\left\langle C_{\rm D}^{-1} \right\rangle + \gamma \left\langle \frac{B}{AC_{\rm D}} \right\rangle \right]^{-1} + \mathcal{O}\left(\omega^{2}\right), \quad \text{where } \gamma = \left\langle \frac{B}{AC_{\rm D}} \right\rangle \left\langle \frac{C}{AC_{\rm D}} \right\rangle^{-1}, \tag{41b}$$

$$\tilde{A} = \left[\left\langle A^{-1} \right\rangle - \left\langle \frac{B^2}{A^2 C_D} \right\rangle + \left\langle C_D^{-1} \right\rangle^{-1} \left\langle \frac{B}{A C_D} \right\rangle^2 \right]^{-1} + \mathcal{O}\left(\omega^2\right), \tag{41c}$$

$$\tilde{B} = \left\langle \frac{B}{AC_{\rm D}} \right\rangle \left[\left\langle A^{-1} \right\rangle \left\langle C_{\rm D}^{-1} \right\rangle - l^{-2} \sum_{p=1}^{2} \sum_{q=p+1}^{3} \frac{l_{p} l_{q}}{C_{\rm Dp} C_{\rm Dq}} \left(\Delta_{qp} \left(\frac{B}{A} \right) \right)^{2} \right]^{-1} + \mathcal{O}\left(\omega^{2}\right), \tag{41d}$$

$$\tilde{S} = \frac{\mathrm{i}\omega}{2l}\tilde{C}\sum_{p=1}^{2}\sum_{q=p+1}^{3}\frac{l_{p}l_{q}}{C_{\mathrm{D}p}C_{\mathrm{D}q}}\left[\Delta_{qp}\left(Z_{D}^{2}\right) + \gamma\frac{B_{p}B_{q}}{A_{p}A_{q}}\Delta_{qp}\left(\frac{A}{B}Z_{D}^{2}\right)\right] + \mathcal{O}\left(\omega^{2}\right),\tag{41e}$$

$$\tilde{W} = \frac{\mathrm{i}\omega}{2l^2} \frac{\tilde{B}}{\left\langle \frac{B}{AC_{\mathrm{D}}} \right\rangle} \sum_{p=1}^{2} \sum_{q=p+1}^{3} \frac{l_p l_q}{C_{\mathrm{D}p} C_{\mathrm{D}q}} \Delta_{qp} \left(\frac{B}{A} \right) \sum_{r=p}^{q} \rho_r l_r \left(2 - \delta_{pr} - \delta_{qr} \right) + \mathcal{O} \left(\omega^2 \right), \tag{41f}$$

where $\delta_{pr}=1$ if p=r, and zero otherwise. We observe that the leading term of all the effective properties except \tilde{S} and \tilde{W} is independent of ω and the ordering of the layers. These terms agree with their expected values from static homogenization in the limiting decoupled case. Thus, the mass density reduces to the arithmetic mean, while when B=0 the stiffness and the permittivity reduce to the harmonic mean.

In contrast, the leading term in the expansions of the Willis coupling and the electromomentum coupling is pure imaginary and linear in ω . Furthermore it depends on the ordering of the layers, such that \tilde{S} and \tilde{W} flip sign when layers 1 and 3 are interchanged. Since these couplings capture the reflection asymmetry, they inherit the dependency on the asymmetry in the electromechanical properties of the scatterer that Eq. (40b) exhibits. We also note that Eq. (40b) can be manipulated to a form that depends explicitly on Z_F and ρB of each layer, with which \tilde{S} can be written as

$$\tilde{S} = \frac{i\omega}{2l} \chi \left\{ l_1 l_2 \left[\alpha_3 \Delta_{21}(Z_E^2) + \beta_3 \Delta_{21}(B\rho) + \frac{A_2 B_1 l_3}{\rho_3} \left(B_1 \rho_1 C_3 \rho_3 - B_3 \rho_3 C_2 \rho_2 \right) + \frac{A_1 B_2 l_3}{\rho_3} \left(B_3 \rho_3 C_1 \rho_1 - B_2 \rho_2 C_3 \rho_3 \right) \right]
+ l_1 l_3 \left[\alpha_2 \Delta_{31}(Z_E^2) + \beta_2 \Delta_{31}(B\rho) + \frac{A_3 B_1 l_2}{\rho_2} \left(B_1 \rho_1 C_2 \rho_2 - B_2 \rho_2 C_3 \rho_3 \right) + \frac{A_1 B_3 l_2}{\rho_2} \left(B_2 \rho_2 C_1 \rho_1 - B_3 \rho_3 C_2 \rho_2 \right) \right]
+ l_2 l_3 \left[\alpha_1 \Delta_{32}(Z_E^2) + \beta_1 \Delta_{32}(B\rho) + \frac{A_3 B_2 l_1}{\rho_1} \left(B_2 \rho_2 C_1 \rho_1 - B_1 \rho_1 C_3 \rho_3 \right) + \frac{A_2 B_3 l_1}{\rho_1} \left(B_1 \rho_1 C_2 \rho_2 - B_3 \rho_3 C_1 \rho_1 \right) \right] \right\}
+ \mathcal{O}\left(\omega^2\right), \tag{42}$$

with some property-dependent constants $\{\chi, \alpha_j, \beta_j, j = 1, 2, 3\}$ that are given in Appendix C. Eq. (42) explicitly shows that \tilde{S} depends on the asymmetry in the elastic impedance $Z_E^2 = \rho C$ and a kind of "piezoelectric impedance": ρB . This expression nicely reduces to an expression that depends only on the elastic impedance when B is zero.

¹⁰ We used Wolfram Mathematica Series function.

5.2.1. Reduction to two lavers

When a scattering element with two layers is used to construct a periodic bulk material, it will always have inversion symmetry. Therefore, to generate \tilde{S} and \tilde{W} Pernas-Salomón and Shmuel [38] broke spatial symmetry in their one-dimensional example using a periodic cell that is made of three layers. To enable a comparison with previous work, we have considered here a three-layer stack in the present work. (Note that our calculations show that in the low frequency regime, the effective properties \tilde{C} , $\tilde{\rho}$, \tilde{B} and \tilde{A} for three-layer elements and their periodic counterpart are the same.) However, it is clear that a two-layer scatterer in a background medium is sufficient to break inversion symmetry, and that expressions for bilayer elements are obtained as a particular case of the above results by setting $l_3=0$. In that case, the expressions for \tilde{C} , $\tilde{\rho}$, \tilde{A} , and \tilde{B} remain the same, only now the averaging is over two layers. The expressions for \tilde{S} and \tilde{W} , on the other hand, simplify to the following expressions

$$\tilde{S} = \frac{\mathrm{i}\omega}{2l} \tilde{C} \frac{l_1 l_2 \left[A_1 A_2 \left\langle A^{-1} \right\rangle \Delta_{21} \left(Z_E^2 \right) + B_1 B_2 \left\langle B^{-1} \right\rangle \Delta_{21} \left(B \rho \right) \right]}{A_1 A_2 C_{\mathrm{D1}} C_{\mathrm{D2}} \left\langle \frac{C}{A C_{\mathrm{D}}} \right\rangle} + \mathcal{O}\left(\omega^2\right), \tag{43a}$$

$$\tilde{W} = \frac{\mathrm{i}\omega}{2l}\tilde{B}\frac{l_1l_2\langle\rho\rangle\,\Delta_{21}\left(\frac{B}{A}\right)}{C_{\mathrm{D1}}C_{\mathrm{D2}}\left(\frac{B}{AC_{\mathrm{D}}}\right)} + \mathcal{O}\left(\omega^2\right). \tag{43b}$$

Eq. (43) reproduces the same functional dependency of \tilde{S} and \tilde{W} as the three-layer expressions, in a simpler form. Eq. (43a) shows that the Willis coupling depends on the asymmetry in the elastic impedance, ρC , as it is well known from the elastic case, and on the asymmetry in the piezoelectric-like impedance, ρB . Eq. (43b) shows that the electromomentum coupling depends on the asymmetry in the ratio between the piezoelectric coefficient and the permittivity, B/A. Notably, the sign of \tilde{S} and \tilde{W} changes when the ordering of the layers is reversed with respect to the coordinate system, since $\Delta_{12}(\cdot) = -\Delta_{12}(\cdot)$.

The fact that \tilde{S} and \tilde{W} depend on asymmetries of different physical quantities has a very important implication: certain compositions of the piezoelectric element may exhibit zero Willis coupling and finite electromomentum coupling. This implies that using such compositions, we can turn on and off the directional phase asymmetry by the opening and closing the circuit, respectively. One such design rule is $\rho_1 C_1 = \rho_2 C_2$, $\rho_1 B_1 = \rho_2 B_2$ and $B_1 A_1^{-1} \neq B_2 A_2^{-1}$. We note that we have implemented this design rule (i.e., ρC and ρB are spatially constant) for a trilayer periodic medium in the rigorous periodic homogenization scheme of Ref. [38]. Interestingly, we found that it also works in the low frequency regime of the periodic case, namely, we received a zero Willis coupling and a nonzero the electromomentum coupling.

5.2.2. Generalization to an arbitrary number of layers and the continuous limit

The low frequency expressions of Eq. (41) for $\tilde{\rho}$, \tilde{C} , \tilde{A} , \tilde{B} , \tilde{S} and \tilde{W} can be generalized to the case of an arbitrary number of n>3 layers. The only change needed is to replace the upper limits, 2 and 3, of the sums over p and q in Eq. (41) by n-1 and n, respectively. The continuous limit, i.e., when the properties of the element vary smoothly $[f_p \to f(x)]$, corresponds to $n \to \infty$, in which case the sums are replaced by integrals and the average of a continuous property is simply $\langle f \rangle = l^{-1} \int_0^1 f \, dx$. In summary, in the continuous limit $\tilde{\rho}$, \tilde{C} and \tilde{A} are exactly as shown in Eq. (41), while the expressions for \tilde{B} , \tilde{S} and \tilde{W} are replaced by

$$\tilde{B} = \left\langle \frac{B}{AC_{\rm D}} \right\rangle \left[\left\langle A^{-1} \right\rangle \left\langle C_{\rm D}^{-1} \right\rangle - l^{-2} \int_{0}^{l} \frac{\mathrm{d}x}{C_{\rm D}(x)} \int_{x}^{l} \frac{\mathrm{d}y}{C_{\rm D}(y)} \left(\frac{B(x)}{A(x)} - \frac{B(y)}{A(y)} \right)^{2} \right]^{-1} + \mathcal{O}\left(\omega^{2}\right), \tag{44a}$$

$$\tilde{S} = -i\omega l\tilde{C} \left\langle \left\langle \rho_{D}, \frac{1}{2C_{D}} \left(1 + \gamma \frac{B}{A} \right) \right\rangle \right\rangle + \mathcal{O}\left(\omega^{2}\right), \tag{44b}$$

$$\tilde{W} = \frac{\mathrm{i}\omega}{l^2} \frac{\tilde{B}}{\left\langle \frac{B}{AC_{\mathrm{D}}} \right\rangle} \int_0^l \frac{\mathrm{d}x}{C_{\mathrm{D}}(x)} \int_x^l \frac{\mathrm{d}y}{C_{\mathrm{D}}(y)} \left(\frac{B(x)}{A(x)} - \frac{B(y)}{A(y)} \right) \int_x^y \rho(z) \mathrm{d}z + \mathcal{O}\left(\omega^2\right), \tag{44c}$$

where the double average $\langle \langle f, g \rangle \rangle$ of two material functions f and g is defined as

$$\langle \langle f, g \rangle \rangle = l^{-2} \int_{0}^{l} f(x) \, \mathrm{d}x \, \int_{0}^{x} g(y) \, \mathrm{d}y - l^{-2} \int_{0}^{l} g(x) \, \mathrm{d}x \, \int_{0}^{x} f(y) \, \mathrm{d}y. \tag{45}$$

Note that the double average is asymmetric in the two material parameters: $\langle\langle f,g\rangle\rangle=-\langle\langle g,f\rangle\rangle$. Also, the identity $Z_D^2=\rho_DC_D$ has been used to simplify \tilde{S} in Eq. (44b). From the above expressions for an arbitrary number of layers, we further deduce that elements made of a repetition

From the above expressions for an arbitrary number of layers, we further deduce that elements made of a repetition of a certain unit cell have the same low-frequency effective properties, independently of the number of cells used to construct them. This is due to the fact that these expressions have the form of volume averages that remain invariant under addition of the same cell to the element. This conclusion is evident from the expressions for $\tilde{\rho}$, \tilde{C} and \tilde{A} , and less evident – but still holds – for the other moduli, as we also observed in a numerical study provided in Appendix D.

Table 1Physical properties of the materials that are used in the computations as the constituents of the element.

Material	C (GPa)	$\rho (kg/m^3)$	$B(C/m^2)$	A (nF/m)
PZT4	115	7500	15.1	5.6
BaTiO ₃	165	6020	3.64	0.97
PVDF	12	1780	-0.027	0.067
PMMA	3.3	1188	0	0.023
Fictitious phase	143.27	6020	18.81	0.97

5.2.3. The source of the directional imaginary part of \tilde{B}^{eq}

Using low frequency expansions, we can also explicitly identify the source of the directional imaginary part of \tilde{B}^{eq} . To this end, we expand Eq. (31) in power series about $\omega = 0$, and obtain the low frequency approximation

$$\tilde{B}_{1}^{\text{eq}} = \tilde{B} - \tilde{W}\tilde{B}\gamma^{-1}Z_{0}^{-1}, \quad \tilde{B}_{R}^{\text{eq}} = \tilde{B} + \tilde{W}\tilde{B}\gamma^{-1}Z_{0}^{-1},$$
(46)

where \tilde{B} and \tilde{W} are given in Eqs. (41d) and (41f), respectively. Thus, \tilde{B}^{eq} is a sum of a real quantity (\tilde{B}) and an imaginary quantity (\tilde{W}), where the latter multiplies a sign that depends on the incident wave direction. Thus, for the *equivalent* model to recover the scattering response of the element, it must absorb the directional phase change that \tilde{W} models into \tilde{B}^{eq} , thereby leading to a piezoelectric coefficient that violates reciprocity and energy conservation. (For similar absorbance of a Willis coupling into an *equivalent* property see Eq. (20) in Ref. [34]. Indeed, the resultant equivalent properties there – although not referred to as such there – violate causality.)

6. Numerical experiments

In this Section, we apply the procedure in Section 4 to numerically calculate the effective properties of two different piezoelectric elements connecting two elastic waveguides made of PMMA. The physical properties of the PMMA, as well as the piezoelectric layers to be considered are given in Table 1. All the calculations to follow are presented as functions of frequency $f = \omega/2\pi$ over the range $0-20\,\mathrm{kHz}$, in which we have found that the low frequency expansions and the original expressions practically coincide. (The difference is less than 0.1%.)

In the first example, we demonstrate the calculation of \tilde{W} , and show that when the element (or, equivalently, the coordinate system) is inverted, the electromomentum modulus changes sign, as it should, since it models an anisotropic material response and hence its value depends on the coordinate system. We show that together with this modulus, the effective properties are physically admissible; by contrast, we show that the *equivalent* properties of the element, albeit recover the same scattering, are physically invalid since they violate energy conservation and reciprocity. The second example not only provides another demonstration of the above observations, but also exhibits a distinctive inconsistency in the retrieved Willis modulus when using the *equivalent* model.

The first element that we analyze is made of 2.62 mm PZT4 (layer 1), 0.19 mm BaTiO₃ (layer 2) and 0.19 mm PVDF (layer 3). As mentioned, we also analyze the properties that are retrieved when the element is inverted (or rotated 180°), i.e., when layers 1 and 3 are interchanged. Fig. 2(a) shows the pure imaginary Willis coupling. Values retrieved from the element ($\tilde{S}^{\triangleright}$, black squares) and its inversion ($\tilde{S}^{\triangleleft}$, blue squares) satisfy $\tilde{S}^{\triangleright} = -\tilde{S}^{\triangleleft}$. Fig. 2(b) shows the pure imaginary electromomentum coupling. Like \tilde{S} , \tilde{W} depends on the orientation (or polarization) of the element: values retrieved from the element ($\tilde{W}^{\triangleright}$, black circles) and its inversion ($\tilde{W}^{\triangleleft}$, blue circles) satisfy $\tilde{W}^{\triangleright} = -\tilde{W}^{\triangleleft}$. Again, we note that this result is consistent with the fact that these moduli model a direction-dependent material response, hence depend on the orientation of the element, or, equivalently, the orientation of the coordinate system.

Fig. 2(c) presents the values of the standard effective properties, where each property is normalized by its arithmetic mean (normalized properties are denoted by overhead hat). Specifically, the brown, red, green and black curves correspond to $\hat{\rho}$, \hat{C} , \hat{A} and \hat{B} , respectively. The computation delivers real constants that are independent of the direction of the incident wave, orientation of the element and the circuit conditions. As such, the effective properties are physically admissible.

We compute next the *equivalent* properties, based on the model that ignores the electromomentum coupling, in order to demonstrate that this model delivers unphysical moduli. To show this, it is sufficient to examine the retrieved piezoelectric coefficient \tilde{B}^{eq} as per the short circuit experiment [Eq. (31)], denoted \tilde{B}^{eq}_s . In this case, the *equivalent* piezoelectric modulus also depends on the direction of the incoming waves, hence we denote values extracted from the fields that are generated by leftward- and rightward incoming waves by $\tilde{B}^{\text{eq}}_{sL}$ and $\tilde{B}^{\text{eq}}_{sR}$, respectively. Results are shown in Fig. 2(d), which depicts the real and imaginary parts of $\tilde{B}^{\text{eq}}_{sL}$ ($\tilde{B}^{\text{eq}}_{sR}$) by the gray (blue) curve and green (red) diamonds, respectively. Indeed, in contrast with the purely real, direction-independent value of \tilde{B} , we observe that \tilde{B}^{eq}_s is a complex-valued, direction-dependent function, as $\tilde{B}^{\text{eq}}_{sL}$ has an imaginary part that is different from the imaginary part of $\tilde{B}^{\text{eq}}_{sR}$. The existence of an imaginary part in the *equivalent* piezoelectric modulus violates energy conservation, while the dependency of the modulus on direction of the incoming wave violates reciprocity. This violation occurs because \tilde{B}^{eq}_s erroneously subsumes the directional phase change that the electromomentum modulus models. Hence, the *equivalent* properties lose their physical meaning, even though they recover the scattering response of the element in the short circuit experiment.

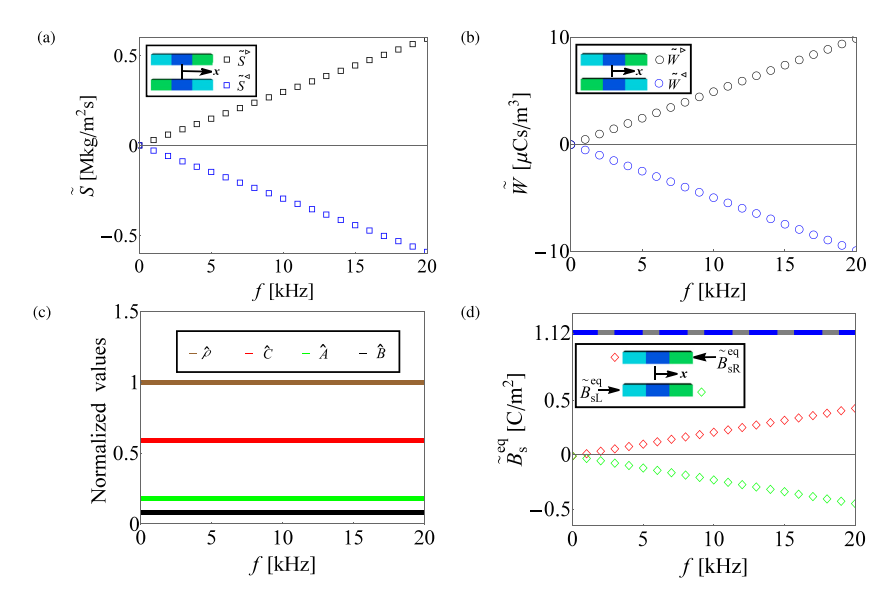


Fig. 2. Retrieved properties of the PZT4-BaTiO-PVDF element and its inversion (see insets) as functions of frequency. (a) The pure imaginary Willis coupling. Values retrieved from the element (\tilde{S}° , black squares) and its inversion (\tilde{S}° , blue squares) satisfy $\tilde{S}^{\circ} = -\tilde{S}^{\circ}$. (b) The pure imaginary electromomentum coupling. Values retrieved from the element (\tilde{W}° , black circles) and its inversion (\tilde{W}° , blue circles) satisfy $\tilde{W}^{\circ} = -\tilde{W}^{\circ}$. (c) The standard effective properties, each one is normalized by its arithmetic mean. Brown, red, green and black curves correspond to $\hat{\rho}$, \hat{C} , \hat{A} and \hat{B} , respectively. (d) The equivalent piezoelectric coefficient $\tilde{B}^{\rm eq}$ that is retrieved from the short circuit experiment. Values extracted from the fields that are generated by leftward- and rightward incident waves are denoted by $\tilde{B}^{\rm eq}_{\rm sl}$ and $\tilde{B}^{\rm eq}_{\rm sR}$, respectively. While Re $\tilde{B}^{\rm eq}_{\rm sl}$ (blue curve) is equal to Re $\tilde{B}^{\rm eq}_{\rm sR}$ (gray curve), we observe that Im $\tilde{B}^{\rm eq}_{\rm sl}$ (green diamond marks) is nonzero and different from Im $\tilde{B}^{\rm eq}_{\rm sR}$ (red diamond marks), thereby violating energy conservation and reciprocity. (For interpretation of the references to color in this figure legend, the reader is referred to the web version of this article.)

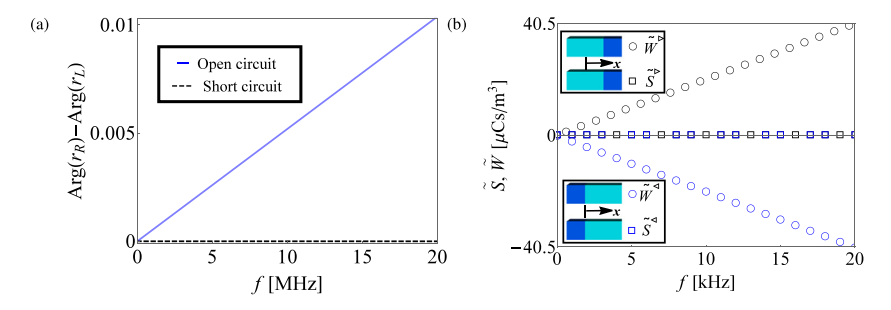


Fig. 3. (a) The difference between the phase of the right (r_R) and left (r_L) reflection coefficients in the open circuit (solid blue line) and short circuit (dashed black line) experiments on the bilayer. According to our design rule, the former is nonzero and the latter is zero. (b) The effective Willis modulus \tilde{S} and electromomentum modulus \tilde{W} of the element. Same legend as in Fig. 2. The modulus \tilde{S} is null, since the right- and left reflection coefficients in the short circuit experiment are equal. The modulus \tilde{W} is a nonzero, pure imaginary function, since the right- and left reflection coefficients in the open circuit experiment differ by a phase, while $\tilde{S} = 0$.

As mentioned previously, there is another inconsistency in the *equivalent* model: the Willis modulus that the *equivalent* model retrieves from the short circuit experiment is different from the value that the *equivalent* model retrieves for the open circuit experiment. For this piezoelectric element, the difference between the two results is minor and not presented here. Essentially, this difference is proportional to the difference in the directional phase change in the two experiments. To demonstrate that this difference can be prominent, in the second example we make use of the conclusion in Section 5, namely, that \tilde{S} is zero when ρC and ρB are constant in the element, and that \tilde{W} is nonzero when B/A is asymmetric in the element. Accordingly, the second element that we consider is a bilayer made of 1.5 mm PZT4 and a 1.5 mm of an artificial material, the properties of which are set according to the above rule (see Table 1 for the specific values). While the properties of the second constituent are fictitious, they are close to the properties of real materials, and guide the selection of available constituents when the objective is to design a real element that will approximate this artificial one.

We present first in Fig. 3(a) the difference in the phase of the right (r_R) and left (r_L) reflection coefficients in the open circuit (solid blue line) and short circuit (dashed black line) experiments on the bilayer. Indeed, following our design rule, the phase of the two reflection coefficients is the same only when the circuit is shorted. We present next in Fig. 3(b) the retrieved effective \tilde{S} and \tilde{W} of the element, as well as of the inverted element (same legend as in Fig. 2) The computation

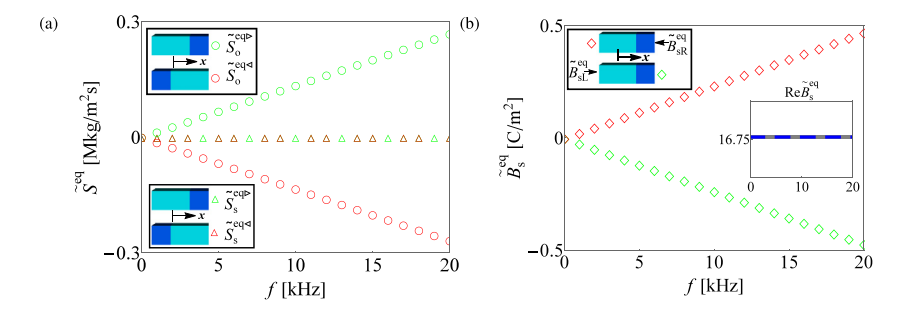


Fig. 4. Retrieved equivalent properties of the bilayer. (a) The pure imaginary \tilde{S}^{eq} as retrieved for the element (green markers) and its inversion (red markers) when the circuit is open (\tilde{S}^{eq}_o , circle marks) and shorted (\tilde{S}^{eq}_s , triangle marks). The fact that $\tilde{S}^{eq}_s \neq \tilde{S}^{eq}_o$ implies that the equivalent model is inconsistent. (b) The equivalent piezoelectric coefficient \tilde{B}^{eq}_s that is retrieved from the short circuit experiment. Same legend as in Fig. 2. Again, the direction-dependent imaginary part of \tilde{B}^{eq} is a violation of reciprocity and energy conservation. (For interpretation of the references to color in this figure legend, the reader is referred to the web version of this article.)

shows that \tilde{S} is null, since the right and left reflection coefficients in the short circuit experiment are equal. By contrast, the modulus \tilde{W} is a nonzero, purely imaginary function, since r_R and r_L in the open circuit experiment differ by a phase, while $\tilde{S}=0$. Before we proceed to analyze the *equivalent* properties of the element, we note that the electromomentum modulus of the element is opposite in sign to the electromomentum modulus of the inverted element, as in the first example.

The Willis modulus that is retrieved from the short circuit experiment using the *equivalent* model (\tilde{S}_s^{eq}) is denoted in Fig. 4(a) by triangle marks, where the green and red colors denote the element and its inversion, respectively. As per our analysis in Section 4, the electromomentum effect is not apparent under short circuit conditions, and hence the *equivalent* Willis modulus that is retrieved in this setting coincides with the effective modulus. Specifically, for this element – which does not generate a phase difference in the short circuit experiment – both models retrieve a null Willis coefficient. However, since there is a phase difference between the reflection coefficients in the open circuit experiment, the *equivalent* model will need a nonzero \tilde{S}^{eq} to capture this. The retrieved values of the *equivalent* model in the open circuit experiment (\tilde{S}_0^{eq}) are denoted in Fig. 4(a) by circle marks. As expected, we observe that \tilde{S}_0^{eq} is different from \tilde{S}_s^{eq} : the latter is identically zero and the former is not. This discrepancy provides further evidence for the need to include the electromomentum modulus in the homogenized constitutive relations.

We conclude the analysis of this element by showing that the *equivalent* model also fails in retrieving a physical piezoelectric modulus, as in the example of the first element. This is demonstrated in Fig. 4(b), which shows the calculation of \tilde{B}_s^{eq} that is extracted from the short circuit experiment [Eq. (31)] (same legend as in Fig. 2). Again, the *equivalent* piezoelectric modulus has an imaginary part, hence does not respect energy conservation. Moreover, this imaginary part depends on the direction of the incident waves, hence it does not respect reciprocity either.

Finally, before summarizing the results of this work, we refer the reader to Appendix D, where we numerically evaluate the exact expressions (i.e., before applying the Taylor approximation) of different elements made of a repetition of the trilayer considered in Fig. 2.

7. Summary

By adapting the homogenization theory of Willis [21–25] to piezoelectric composites, Pernas-Salomón and Shmuel [38] have found that a macroscopic cross-coupling between the momentum and electric field emerges if the media has broken inversion symmetry. The electromomentum coupling constitutes an additional degree of freedom in the design space of metamaterials, which reflects an unusual interplay between the kinetic energy and electric energy at the macroscale. The objective of this work was to provide a heuristic demonstration of this coupling, analyze its effect, and elucidate its physical origins.

Towards this end, we have analyzed first the effect of the electromomentum coupling on plane waves in homogenized media under short circuit and open circuit conditions. This analysis shows that only under open circuit conditions, the coupling modifies the phase velocity and introduces a directional phase angle to the characteristic elastic impedance. The former feature is similar to the effect that the piezoelectric coupling has on the phase velocity, and the latter feature is similar to the effect that the Willis coupling has on the characteristic impedance.

The analysis suggests that these features can be quantified from the scattering properties of a one-dimensional asymmetric piezoelectric scatterer. To do so, we have calculated analytically its scattering coefficients in response to rightward- and leftward incident waves, under the two circuit conditions. We then used an inverse program to determine the properties of a homogenized medium according to two models: an *effective* model that includes both Willis and electromomentum coupling, and an *equivalent* model that neglects electromomentum coupling [10,18,47]. This heuristic

homogenization approach is applicable only in the long-wavelength, low frequency regime [1]. The conclusions that we have found and demonstrated numerically correspond to this limit, are summarized next.

We highlight the main observation from this analysis: the reflection of rightward- and leftward incident waves is different by a phase, where this phase depends on the electric circuit conditions, i.e., if the circuit is shorted or open. It is precisely the extra phase in the open circuit that only the electromomentum coupling captures. Together with this coupling, the properties that are retrieved from the scattering experiments using the effective model satisfy reciprocity and energy conservation, and are independent of the excitation setup. By contrast, the properties of the *equivalent* model that are retrieved from the short circuit setup violate reciprocity and energy conservation, and are different from the values that are retrieved from the open circuit setup, even in the low frequency regime. We note that such violations of physical laws by *equivalent* models that neglect the electromomentum coupling were also found in studies of infinite piezoelectric media using rigorous homogenization, based on ensemble averaging, see Ref. [35].

We have obtained explicit expressions for the low frequency approximations of the effective properties of element with an arbitrary number of layers using Taylor expansions. These expressions show that elements that are made of a repetition of a certain unit cell have the same effective properties at low frequencies, independently of the number of cells used to construct those elements. The leading term in the expansions of the effective mass, stiffness and permittivity is a real constant that agrees with their expected value from static homogenization in the limiting decoupled case. By contrast, the leading term in the expansions of the Willis coupling and the electromomentum coupling is a linear function of the frequency, and purely imaginary, hence responsible for the phase change. The expansion of the former clearly shows that the Willis coupling depends on the asymmetry in the impedance – as known in the elastic case – and the asymmetry in a kind of a piezoelectric impedance, that is the product of the piezoelectric coefficient by the mass density. The leading term in the expansion of the electromomentum coupling depends on the asymmetry in the ratio between the piezoelectric constant and the permittivity. Hence, it is possible to design elements that have zero Willis coupling and finite electromomentum coupling. The directional phase angle of such element vanishes in the short circuit setup – since it depends only on the Willis coupling – and persists in the open circuit setup since it depends on the electromomentum coupling. This observation suggests a convenient way to control the directional phase change by the opening and shorting of the circuit.

We expect the demonstration of the electromomentum effect in this simple setting to promote further studies of its implications in more general settings, and its engineering for applications that require control over elastic waves.

CRediT authorship contribution statement

René Pernas-Salomón: Methodology, Software, Formal analysis, Validation, Investigation, Writing - original draft, Writing - review & editing, Visualization. **Michael R. Haberman:** Formal analysis, Investigation, Writing - original draft, Writing - review & editing, Visualization. **Andrew N. Norris:** Formal analysis, Investigation, Writing - original draft, Writing - review & editing, Visualization. **Gal Shmuel:** Conceptualization, Methodology, Investigation, Writing - original draft, Writing - review & editing, Visualization, Supervision, Funding acquisition.

Declaration of competing interest

The authors declare that they have no known competing financial interests or personal relationships that could have appeared to influence the work reported in this paper.

Acknowledgments

We thank anonymous reviewers for useful comments that helped us improve this paper. This research was supported by the Israel Science Foundation, funded by the Israel Academy of Sciences and Humanities (Grant no. 2061/20), the United States-Israel Binational Science Foundation (Grant no. 2014358), and Ministry of Science and Technology, Israel (Grant no. 880011). A.N.N. and M.R.H. acknowledge support from NSF EFRI, USA award no. 1641078 and M.R.H. acknowledges additional support ONR YIP, USA award no. N00014-18-1-2335.

Appendix A. The transfer matrix for the mechanical fields of the homogenized medium in short circuit

Consider a finite slab of homogeneous medium governed by Eq. (3), admitting plane waves of the form $u(x,t) = Ue^{\pm i \bar{k}_E x - i \omega t}$. In a short circuit configuration such that the electric field vanishes, its stress and momentum reduce to the Willis form

$$\sigma = \tilde{C}u_{,x} - i\omega \tilde{S}u,\tag{A.1}$$

$$p = \tilde{S}^{\dagger} u_{x} - i\omega \tilde{\rho} u. \tag{A.2}$$

We extract the strain from Eq. (A.1):

$$u_{,x} = \tilde{C}^{-1}\sigma + i\omega\tilde{S}\tilde{C}^{-1}u,\tag{A.3}$$

substitute it into Eq. (A.2), and then use the resultant expression for p in the governing equation $\sigma_{x} = -i\omega p$ to obtain

$$\sigma_{,x} = -i\omega \tilde{S}^{\dagger} \tilde{C}^{-1} \sigma + \omega^2 \left(\tilde{S} \tilde{S}^{\dagger} \tilde{C}^{-1} - \tilde{\rho} \right) u. \tag{A.4}$$

Eq. (A.3)) and (A.4) are written in matrix form as

$$\begin{pmatrix} u_{,x} \\ \sigma_{,x} \end{pmatrix} = \mathbf{M} \begin{pmatrix} u \\ \sigma \end{pmatrix} \text{ where } \mathbf{M} = \begin{pmatrix} i\omega \tilde{S}\tilde{C}^{-1} & \tilde{C}^{-1} \\ \omega^2 (\tilde{S}\tilde{S}^{\dagger}\tilde{C}^{-1} - \tilde{\rho}) & -i\omega \tilde{S}^{\dagger}\tilde{C}^{-1} \end{pmatrix}.$$
 (A.5)

Considering plane wave solutions, Eq. (A.5) leads to the following relation between the displacement and stress at two different points in the slab:

$$\begin{pmatrix} u(x_b) \\ \sigma(x_b) \end{pmatrix} = \mathsf{T}^{\mathsf{m}}(x_b, x_a) \begin{pmatrix} u(x_a) \\ \sigma(x_a) \end{pmatrix}, \quad x_0 \le x_a, x_b \le x_3, \tag{A.6}$$

where

$$\mathsf{T}^{\mathsf{m}}(\mathsf{x}_b,\mathsf{x}_a) = e^{(\mathsf{x}_b - \mathsf{x}_a)\mathsf{M}} \tag{A.7}$$

is the transfer matrix relating the displacement and stress fields at the space coordinates x_a and x_b .

Appendix B. Retrieved properties in the clamped ends configuration

This appendix provides an analysis of a third setup that verifies the consistency of the effective properties. We consider a setup with zero average strain by clamping the ends x_0 and x_3 , and excite the stack by applying a time harmonic $(e^{-i\omega t})$ voltage drop. (This configuration is consistent with an effective stress-charge form since we evaluate the effective permittivity and piezoelectric coefficients at a prescribed effective strain when an electric field generates stress and electric displacement field.)

We determine the effective properties from the requirement that the fictitious medium will deliver the same average fields as in the piezoelectric stack. To this end, we first calculate the exact fields in the stack, as follows. From Eq. (15) we obtain

$$\sigma(x_0) = -\frac{T_{14}^{\triangleright}}{T_{12}^{\triangleright}}D,\tag{B.1}$$

which together with Eqs. (14) and (B.1) determine u(x) and $\sigma(x)$ as

$$u(x) = \begin{cases} D\left(\frac{B_{1}}{A_{1}} - \frac{T_{14}^{\triangleright}}{T_{13}^{\triangleright}}\right) \frac{\sin k_{D1} (x - x_{0})}{\omega Z_{D1}}, & x_{0} \leq x \leq x_{1}, \\ u(x_{1}) \cos k_{D2} (x - x_{1}) + \left[\sigma (x_{1}) + \frac{B_{2}}{A_{2}}D\right] \frac{\sin k_{D2} (x - x_{1})}{\omega Z_{D2}}, & x_{1} \leq x \leq x_{2}, \\ u(x_{2}) \cos k_{D3} (x - x_{2}) + \left[\sigma (x_{2}) + \frac{B_{3}}{A_{3}}D\right] \frac{\sin k_{D3} (x - x_{2})}{\omega Z_{D3}}, & x_{2} \leq x \leq x_{3}, \end{cases}$$
(B.2)

where $T^{\triangleright} = T_3^{em} T_2^{em} T_1^{em}$ and

$$u(x_1) = \left(T_{1(14)}^{\text{em}} - T_{1(13)}^{\text{em}} \frac{T_{14}^{\triangleright}}{T_{13}^{\triangleright}}\right) D, \quad u(x_2) = T_{2(11)}^{\text{em}} u(x_1) + T_{2(13)}^{\text{em}} \sigma(x_1) + T_{2(14)}^{\text{em}} D, \tag{B.3}$$

$$\sigma(x_1) = \left(T_{1(34)}^{\text{em}} - T_{1(33)}^{\text{em}} \frac{T_{14}^{\triangleright}}{T_{13}^{\triangleright}}\right) D, \quad \sigma(x_2) = T_{2(31)}^{\text{em}} u(x_1) + T_{2(33)}^{\text{em}} \sigma(x_1) + T_{2(34)}^{\text{em}} D, \tag{B.4}$$

and $T_{n(ij)}^{\rm em}$ is the ij-component of the matrix $T_n^{\rm em}$. The stress as function of x is $\sigma(x) = C_{Dn}u_{,x} - (B_n/A_n)D$, for $x_{n-1} \le x \le x_n$, n=1,2,3. Furthermore, from Eqs. (15) and (B.1) we have that

$$\phi(x_3) - \phi(x_0) = \left(T_{24}^{\triangleright} - T_{23}^{\triangleright} \frac{T_{14}^{\triangleright}}{T_{12}^{\triangleright}}\right) D. \tag{B.5}$$

Having determined u(x) and $\sigma(x)$ allows us to average over the stack, which together with Eq. (B.5) and the fact that (in absence the of charge) D is constant in the stack provide

$$l\langle u\rangle = \Gamma_1^{\triangleright} \langle D\rangle, \quad l\langle \sigma\rangle = \Gamma_2^{\triangleright} \langle D\rangle, \quad l\langle \phi_{,x}\rangle = \Gamma_3^{\triangleright} \langle D\rangle, \tag{B.6}$$

where the terms $\Gamma_i^{\triangleright}$ are

$$\Gamma_{1}^{\triangleright} = \left(\frac{B_{1}}{A_{1}} - \frac{T_{14}^{\triangleright}}{T_{13}^{\triangleright}}\right) \frac{1 - \cos k_{D1} l_{1}}{\omega k_{D1} Z_{D1}}$$

$$+ \left(T_{1(14)}^{em} - T_{1(13)}^{em} \frac{T_{14}^{\triangleright}}{T_{13}^{\triangleright}}\right) \frac{\sin k_{D2} l_{2}}{k_{D2}} + \left(T_{1(34)}^{em} - T_{1(33)}^{em} \frac{T_{14}^{\triangleright}}{T_{13}^{\triangleright}} + \frac{B_{2}}{A_{2}}\right) \frac{1 - \cos k_{D2} l_{2}}{\omega k_{D2} Z_{D2}}$$

$$+ \left[T_{2(11)}^{em} \left(T_{1(14)}^{em} - T_{1(13)}^{em} \frac{T_{14}^{\triangleright}}{T_{13}^{\triangleright}}\right) + T_{2(13)}^{em} \left(T_{1(34)}^{em} - T_{1(33)}^{em} \frac{T_{14}^{\triangleright}}{T_{13}^{\triangleright}}\right) + T_{2(14)}^{em}\right] \frac{\sin k_{D3} l_{3}}{k_{D3}}$$

$$+ \left[T_{2(31)}^{em} \left(T_{1(14)}^{em} - T_{1(13)}^{em} \frac{T_{14}^{\triangleright}}{T_{13}^{\triangleright}}\right) + T_{2(33)}^{em} \left(T_{1(34)}^{em} - T_{1(33)}^{em} \frac{T_{14}^{\triangleright}}{T_{13}^{\triangleright}}\right) + T_{2(34)}^{em} + \frac{B_{3}}{A_{3}}\right] \frac{1 - \cos k_{D3} l_{3}}{\omega k_{D3} Z_{D3}}$$
(B.7)

$$\begin{split} &\Gamma_{2}^{\triangleright} = \left(\frac{B_{1}}{A_{1}} - \frac{T_{14}^{\triangleright}}{T_{13}^{\triangleright}}\right) \frac{\sin k_{D1} l_{1}}{k_{D1}} - \frac{B_{1}}{A_{1}} l_{1} \\ &+ \left(T_{1(34)}^{em} - T_{1(33)}^{em} \frac{T_{14}^{\triangleright}}{T_{13}^{\triangleright}} + \frac{B_{2}}{A_{2}}\right) \frac{\sin k_{D2} l_{2}}{k_{D2}} - \omega Z_{D2} \left(T_{1(14)}^{em} - T_{1(33)}^{em} \frac{T_{14}^{\triangleright}}{T_{13}^{\triangleright}}\right) \frac{1 - \cos k_{D2} l_{2}}{k_{D2}} - \frac{B_{2}}{A_{2}} l_{2} \\ &+ \left[T_{2(31)}^{em} \left(T_{1(14)}^{em} - T_{1(13)}^{em} \frac{T_{14}^{\triangleright}}{T_{13}^{\triangleright}}\right) + T_{2(33)}^{em} \left(T_{1(34)}^{em} - T_{1(33)}^{em} \frac{T_{14}^{\triangleright}}{T_{13}^{\triangleright}}\right) + T_{2(34)}^{em} + \frac{B_{3}}{A_{3}}\right] \frac{\sin k_{D3} l_{3}}{k_{D3}} \\ &- \omega Z_{D3} \left[T_{2(11)}^{em} \left(T_{1(14)}^{em} - T_{1(13)}^{em} \frac{T_{14}^{\triangleright}}{T_{13}^{\triangleright}}\right) + T_{2(13)}^{em} \left(T_{1(34)}^{em} - T_{1(33)}^{em} \frac{T_{14}^{\triangleright}}{T_{13}^{\triangleright}}\right) + T_{2(14)}^{em}\right] \frac{1 - \cos k_{D3} l_{3}}{k_{D3}} - \frac{B_{3}}{A_{3}} l_{3}, \end{split} \tag{B.8}$$

$$&\Gamma_{3}^{\triangleright} = T_{24}^{\triangleright} - T_{23}^{\triangleright} \frac{T_{14}^{\triangleright}}{T^{\triangleright}}. \tag{B.9}$$

We are now in a position to determine the effective properties from the relations between average fields. Since we use the equations for the average stress and electric displacement field when the average strain is zero, then the retrieved piezoelectric coefficient is the same whether we use \tilde{W} as in model (3), or neglect it as in the *equivalent* model; by contrast, the *equivalent* permittivity is different from the effective permittivity if \tilde{W} is neglected. When \tilde{W} is included, the effective properties read

$$\tilde{A}^{\triangleright} = -\frac{l + i\omega \tilde{W}^{\triangleright} \Gamma_1^{\triangleright}}{\Gamma_3^{\triangleright}}, \quad \tilde{B}^{\triangleright} = \frac{\Gamma_2^{\triangleright} + i\omega \tilde{S}^{\triangleright} \Gamma_1^{\triangleright}}{\Gamma_3^{\triangleright}}; \tag{B.10}$$

here, we use superscript $^{\triangleright}$ to distinguish the results for this element from the results for an inverted element, the layers 1 and 3 of which are interchanged. Eq. (B.10) provides a third equation to determine \tilde{W} . Thus, together with Eq. (35a) we obtain

$$\tilde{W}^{\triangleright} = -\frac{l\left(\tilde{S}_{0}^{\triangleright eq} - \tilde{S}^{\triangleright}\right)}{\Gamma_{2}^{\triangleright} + i\omega\tilde{S}_{0}^{\triangleright eq}\Gamma_{1}^{\triangleright}}$$
(B.11)

where \tilde{S}_0^{peq} equals the right-hand side of Eq. (35a). We note that if \tilde{W} is neglected, then the expressions for the *equivalent* permittivity from this experiment is determined by setting $\tilde{W} = 0$ in Eq. (B.10)₁.

It is straightforward to carry out the same analysis if the element is inverted, i.e., if layers 1 and 3 in the element are interchanged. In this case $\tilde{A}^{\triangleleft}$ and $\tilde{B}^{\triangleleft}$ of the inverted element are given by

$$\tilde{A}^{\triangleleft} = -\frac{l + i\omega \tilde{W}^{\triangleleft} \Gamma_{1}^{\triangleleft}}{\Gamma_{3}^{\triangleleft}}, \quad \tilde{B}^{\triangleleft} = \frac{\Gamma_{2}^{\triangleleft} + i\omega \tilde{S}^{\triangleleft} \Gamma_{1}^{\triangleleft}}{\Gamma_{3}^{\triangleleft}}; \tag{B.12}$$

here, Γ_1^{\triangleleft} , Γ_2^{\triangleleft} and Γ_3^{\triangleleft} correspond to the case where layers 1 and 3 of the laminate are swapped, and can be obtained, respectively, from the expressions for $\Gamma_1^{\triangleright}$, $\Gamma_2^{\triangleright}$ and $\Gamma_3^{\triangleright}$ by interchanging the properties and matrices corresponding to the layers 1 and 3, and replacing the matrix T^{\triangleright} by the matrix $T^{\triangleleft} = T_1^{em} T_2^{em} T_3^{em}$. Again, by substituting Eq. (B.12) into Eq. (35a) we obtain

$$\tilde{W}^{\triangleleft} = -\frac{l\left(\tilde{S}_{o}^{\text{seq}} - \tilde{S}^{\triangleleft}\right)}{\Gamma_{2}^{\square} + i\omega\tilde{S}_{o}^{\text{seq}}\Gamma_{1}^{\square}},\tag{B.13}$$

where $\tilde{S}_0^{\triangleright eq}$ is given by the right-hand side of Eq. (35a) for the inverted element. Now, since Eqs. (14) and (15) verify that $\Gamma_1^{\triangleleft} = -\Gamma_1^{\triangleright}$, $\Gamma_2^{\triangleleft} = \Gamma_2^{\triangleright}$ and $\Gamma_3^{\triangleleft} = \Gamma_3^{\triangleright}$, and Eqs. (28a) and (35a) imply that $\tilde{S}^{\triangleleft} = -\tilde{S}^{\triangleright}$ and $\tilde{S}^{\triangleright eq} = -\tilde{S}^{\triangleleft eq}$, and hence the electromomentum coupling changes sign when the element is inverted, i.e., $\tilde{W}^{\triangleleft} = -\tilde{W}^{\triangleright}$, like the Willis coupling. Together, the former imply that $\tilde{A}^{\triangleright} = \tilde{A}^{\triangleleft}$, $\tilde{B}^{\triangleright} = \tilde{B}^{\triangleleft}$.

The above analysis demonstrates another inconsistency in the *equivalent* model that neglects W: the extracted values for the equivalent piezoelectric coefficients are different in the short circuit experiment and in this experiment,

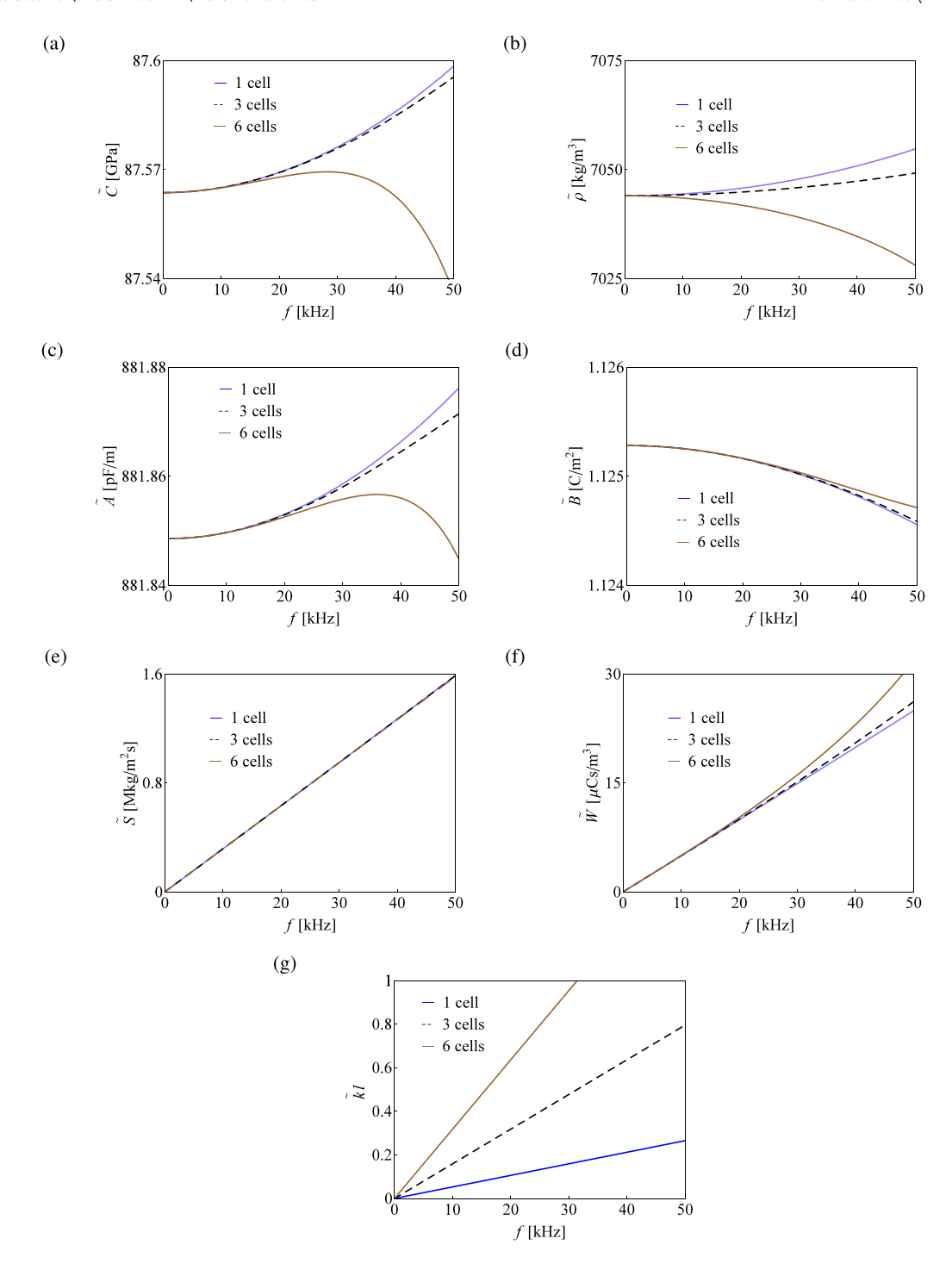


Fig. 5. A comparison of the effective (a) stiffness; (b) mass density; (c) dielectric; (d) piezoelectric; (e) Willis; and (f) electromomentum moduli of elements made of repetitions of the element in the first example. Blue, black and brown correspond to one-, three- and six repetitions. (g) Normalized effective wavenumber of the three elements, $\tilde{k}l$, versus frequency, for the three elements. (For interpretation of the references to color in this figure legend, the reader is referred to the web version of this article.)

i.e., Eqs. (31) and $(B.10)_2$, are different. This is evident from the fact that Eq. (31) is complex-valued, while Eqs. $(B.10)_2$ is real-valued.

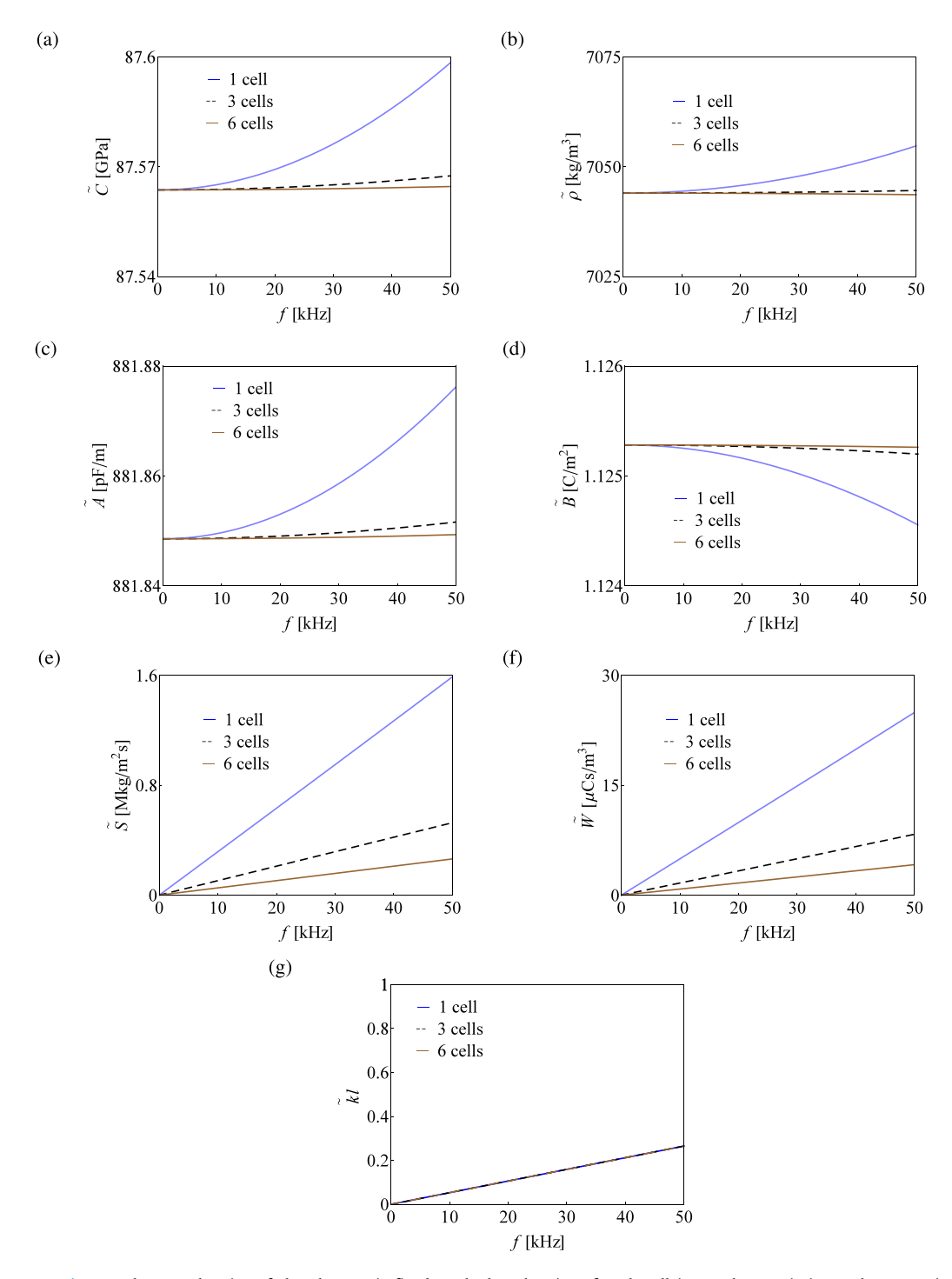


Fig. 6. Same as Fig. 5, only now the size of the element is fixed, such that the size of each cell in an element is inversely proportional to the number of cells in that element.

Appendix C. The coefficients in the alternative expression of \tilde{S}

The constants that appear in Eq. (42) are

$$\chi = (A_1 A_2 C_{D1} C_{D2} C_3 l_3 + A_1 A_3 C_{D1} C_{D3} C_2 l_2 + A_2 A_3 C_{D2} C_{D3} C_1 l_1)^{-1} \tilde{C},$$

and

```
\begin{split} &\alpha_1 = A_2 A_3 C_1 l_1 + A_1 C_{D1} \left( A_2 l_3 + A_3 l_2 \right), \quad \beta_1 = B_1 B_2 B_3 l_1 + A_1 C_{D1} \left( B_3 l_2 + B_2 l_3 \right), \\ &\alpha_2 = A_1 A_3 C_2 l_2 + A_2 C_{D2} \left( A_1 l_3 + A_3 l_1 \right), \quad \beta_2 = B_1 B_2 B_3 l_2 + A_2 C_{D2} \left( B_3 l_1 + B_1 l_3 \right), \\ &\alpha_3 = A_1 A_2 C_3 l_3 + A_3 C_{D3} \left( A_1 l_2 + A_2 l_1 \right), \quad \beta_3 = B_1 B_2 B_3 l_3 + A_3 C_{D3} \left( B_2 l_1 + B_1 l_2 \right). \end{split}
```

Appendix D. A comparison of the effective properties of elements with different number of cells beyond the quasistatic limit

In this Appendix, we numerically evaluate the exact expressions of the effective properties [i.e., those obtained from Eqs. (28),(35) and (38), not the asymptotic expressions] of elements made of a repetition of the trilayer considered in Fig. 2. The purpose is to provide an example, showing that (i) the first-order approximations hold beyond the quasistatic regime ($\tilde{k}a$ <0.01, a being the lattice constant); (ii) the effective properties of different elements made of the same cell are equal, independently of the number of cells used to construct the element. These features are shown in Fig. 5. Specifically, panels 5(a)-5(f) show the effective stiffness, mass density, dielectric-, piezoelectric-, Willis-, and electromomentum moduli of the elements, respectively, as functions of the frequency. Blue, black and brown correspond to one-, three- and six repetitions of the trilayer. We observe that up to a limiting frequency (which is not constant for all moduli), the effective properties of all three elements coincide.

The formal applicability limit of the quasistatic homogenization is usually quantified in terms of the effective wavenumber normalized by the lattice constant, say a, according to $\tilde{k}a < 0.01$ [48]. Since here we do not really have a lattice, only a number of unit cells, we choose to examine the effective wavenumber of the three elements, normalized by the length of each element, i.e., $\tilde{k}l$. This is shown in panel 5(g). We observe that the limit $\tilde{k}l = 0.01$ corresponds to the frequencies 1890 Hz, 630 Hz and 315 Hz, for the elements with one-, three- and six cells, respectively. Notably, the first order approximations hold beyond those frequencies, as we see that the ordinary (resp. the Willis- and electromomentum) moduli in the previous panels are constant (resp. linear) beyond those frequency values. This observation agrees with the results in Ref. [61] for second order homogenization in one-dimensional elastodynamics.

We note that it is the size of the unit cell, *a* that is important in determining the effective properties, not the size of the element. This is shown in Fig. 6, which is the same as Fig. 5, only now the length of all elements are equal, such that the size of each cell in an element is inversely proportional to the number of cells in that element. We observe that now the agreement between effective properties of the different elements is limited to a more narrow range of frequencies. Most notably, the Willis- and electromomentum moduli of the three elements are different at all frequencies, which is consistent with the low-frequency expansions for Willis coupling in acoustics, where the Willis coupling modulus has been shown to depend on the lattice constant [18].

References

- [1] C.R. Simovski, Material parameters of metamaterials (a review), Opt. Spectrosc. 107 (5) (2009) 726, http://dx.doi.org/10.1134/ S0030400X09110101
- [2] Martin Wegener, Metamaterials beyond optics, Science 342 (6161) (2013) 939–940, http://dx.doi.org/10.1126/science.1246545, https://science.sciencemag.org/content/342/6161/939.
- [3] Ankit Srivastava, Elastic metamaterials and dynamic homogenization: a review, Int. J. Smart Nano Mater. 6 (1) (2015) 41–60, http://dx.doi.org/10.1080/19475411.2015.1017779.
- [4] Muamer Kadic, Graeme W. Milton, Martin van Hecke, Martin Wegener, 3D Metamaterials, Nat. Rev. Phys. 1 (3) (2019) 198–210, http://dx.doi.org/10.1038/s42254-018-0018-y.
- [5] Steven A. Cummer, Johan Christensen, Andrea Alù, Controlling sound with acoustic metamaterials, Nat. Rev. Mater. 1 (3) (2016) 1-13.
- [6] Katia Bertoldi, Vincenzo Vitelli, Johan Christensen, Martin van Hecke, Flexible mechanical metamaterials, Nat. Rev. Mater. 2 (11) (2017) 17066.
- [7] Yiqun Ding, Zhengyou Liu, Chunyin Qiu, Jing Shi, Metamaterial with simultaneously negative bulk modulus and mass density, Phys. Rev. Lett. 99 (9) (2007) 93904, http://dx.doi.org/10.1103/PhysRevLett.99.093904.
- [8] X.N. Liu, G.K. Hu, G.L. Huang, C.T. Sun, An elastic metamaterial with simultaneously negative mass density and bulk modulus, Appl. Phys. Lett. 98 (25) (2011) 251907, http://dx.doi.org/10.1063/1.3597651.
- [9] E.B. Duoss, T.H. Weisgraber, K. Hearon, C. Zhu, I.V. W Small, T.R. Metz, J.J. Vericella, H.D. Barth, J.D. Kuntz, R.S. Maxwell, C.M. Spadaccini, T.S. Wilson, Three-dimensional printing of elastomeric, cellular architectures with negative stiffness, Adv. Funct. Mater. 24 (31) (2014) 4905–4913.
- [10] Michael B. Muhlestein, Caleb F. Sieck, Preston S. Wilson, Michael R. Haberman, Experimental evidence of Willis coupling in a one-dimensional effective material element, Nature Commun. 8 (2017) 15625 EP -. https://doi.org/10.1038/ncomms15625.
- [11] Li Quan, Younes Ra'di, Dimitrios L. Sounas, Andrea Alù, Maximum Willis coupling in acoustic scatterers, Phys. Rev. Lett. 120 (25) (2018) 254301, http://dx.doi.org/10.1103/PhysRevLett.120.254301.
- [12] Aurélien Merkel, Vicent Romero-García, Jean-Philippe Groby, Jensen Li, Johan Christensen, Unidirectional zero sonic reflection in passive PT-symmetric Willis media, Phys. Rev. B 98 (2018) 201102, http://dx.doi.org/10.1103/PhysRevB.98.201102.
- [13] Yongquan Liu, Zixian Liang, Jian Zhu, Lingbo Xia, Olivier Mondain-Monval, Thomas Brunet, Andrea Alù, Jensen Li, Willis metamaterial on a structured beam, Phys. Rev. X 9 (2019) 011040, http://dx.doi.org/10.1103/PhysRevX.9.011040.
- [14] Anton Melnikov, Yan Kei Chiang, Li Quan, Sebastian Oberst, Andrea Alù, Steffen Marburg, David Powell, Acoustic meta-atom with experimentally verified maximum Willis coupling, Nature Commun. 10 (1) (2019) 3148, http://dx.doi.org/10.1038/s41467-019-10915-5.
- [15] G.W. Milton, M. Briane, J.R. Willis, On cloaking for elasticity and physical equations with a transformation invariant form, New J. Phys. 8 (10) (2006) 248, http://stacks.iop.org/1367-2630/8/i=10/a=248.
- [16] G.W. Milton, J.R. Willis, On modifications of Newton's second law and linear continuum elastodynamics, Proc. R. Soc. London A Math. Phys. Eng. Sci. 463 (2079) (2007) 855–880, http://dx.doi.org/10.1098/rspa.2006.1795, http://rspa.royalsocietypublishing.org/content/463/2079/855.

- [17] Michael B. Muhlestein, Caleb F. Sieck, Andrea Alù, Michael R. Haberman, Reciprocity, passivity and causality in Willis materials, Proc. R. Soc. London A Math. Phys. Eng. Sci. 472 (2194) (2016) http://dx.doi.org/10.1098/rspa.2016.0604.
- [18] Caleb F. Sieck, Andrea Alù, Michael R. Haberman, Origins of Willis coupling and acoustic bianisotropy in acoustic metamaterials through source-driven homogenization, Phys. Rev. B 96 (10) (2017) 104303, http://dx.doi.org/10.1103/PhysRevB.96.104303.
- [19] Viktar S. Asadchy, Ana Díaz-Rubio, Sergei A. Tretyakov, Bianisotropic metasurfaces: physics and applications, Nanophotonics 7 (6) (2018) 1069–1094.
- [20] M. Albooyeh, V.S. Asadchy, R. Alaee, S.M. Hashemi, M. Yazdi, M.S. Mirmoosa, C. Rockstuhl, C.R. Simovski, S.A. Tretyakov, Purely bianisotropic scatterers, Phys. Rev. B 94 (24) (2016) 245428.
- [21] J.R. Willis, Polarization approach to the scattering of elastic waves—I. scattering by a single inclusion, J. Mech. Phys. Solids 28 (5) (1980) 287–305, http://dx.doi.org/10.1016/0022-5096(80)90021-6, http://www.sciencedirect.com/science/article/pii/0022509680900216.
- [22] J.R. Willis, Variational principles for dynamic problems for inhomogeneous elastic media, Wave Motion 3 (1) (1981) 1–11, http://dx.doi.org/10. 1016/0165-2125(81)90008-1, http://www.sciencedirect.com/science/article/pii/0165212581900081.
- [23] J.R. Willis, The nonlocal influence of density variations in a composite, Int. J. Solids Struct. 21 (7) (1985) 805–817, http://dx.doi.org/10.1016/0020-7683(85)90084-8, http://www.sciencedirect.com/science/article/pii/0020768385900848.
- [24] J.R. Willis, Effective constitutive relations for waves in composites and metamaterials, Proc. R. Soc. London A Math. Phys. Eng. Sci. 467 (2131) (2011) 1865–1879, http://dx.doi.org/10.1098/rspa.2010.0620, http://rspa.royalsocietypublishing.org/content/467/2131/1865.
- [25] John R. Willis, The construction of effective relations for waves in a composite, Comptes Rendus MÉCanique 340 (4) (2012) 181–192, http://dx.doi.org/10.1016/j.crme.2012.02.001, http://www.sciencedirect.com/science/article/pii/S1631072112000381.
- [26] S. Nemat-Nasser, A. Srivastava, Overall dynamic constitutive relations of layered elastic composites, J. Mech. Phys. Solids 59 (10) (2011) 1953–1965, http://dx.doi.org/10.1016/j.jmps.2011.07.008, http://www.sciencedirect.com/science/article/pii/S0022509611001475.
- [27] A.L. Shuvalov, A.A. Kutsenko, A.N. Norris, O Poncelet, Effective Willis constitutive equations for periodically stratified anisotropic elastic media, Proc. R. Soc. London A Math. Phys. Eng. Sci. 467 (2130) (2011) 1749–1769, http://dx.doi.org/10.1098/rspa.2010.0389, http://rspa.royalsocietypublishing.org/content/467/2130/1749.
- [28] A.N. Norris, A.L. Shuvalov, A.A. Kutsenko, Analytical formulation of three-dimensional dynamic homogenization for periodic elastic systems, Proc. R. Soc. London A Math. Phys. Eng. Sci. (2012) http://dx.doi.org/10.1098/rspa.2011.0698, http://rspa.royalsocietypublishing.org/content/early/ 2012/02/14/rspa.2011.0698.
- [29] H. Nassar, Q.-C. He, N. Auffray, Willis elastodynamic homogenization theory revisited for periodic media, J. Mech. Phys. Solids 77 (2015) 158–178, http://dx.doi.org/10.1016/j.jmps.2014.12.011, http://www.sciencedirect.com/science/article/pii/S0022509614002579.
- [30] H. Nassar, Q.-C. He, N. Auffray, On asymptotic elastodynamic homogenization approaches for periodic media, J. Mech. Phys. Solids 88 (2016) 274–290, http://dx.doi.org/10.1016/j.jmps.2015.12.020, http://www.sciencedirect.com/science/article/pii/S0022509615303859.
- [31] Daniel Torrent, Yan Pennec, Bahram Djafari-Rouhani, Resonant and nonlocal properties of phononic metasolids, Phys. Rev. B 92 (17) (2015) 174110, http://dx.doi.org/10.1103/PhysRevB.92.174110.
- [32] Marie-Fraise Ponge, Olivier Poncelet, Daniel Torrent, Dynamic homogenization theory for nonlocal acoustic metamaterials, Extrem. Mech. Lett. 12 (2017) 71–76, http://dx.doi.org/10.1016/j.eml.2016.10.006, http://www.sciencedirect.com/science/article/pii/S2352431616300979.
- 12 (2017) 71–76, http://dx.doi.org/10.1016/j.eml.2016.10.006, http://www.sciencedirect.com/science/article/pii/S2352431616300979.

 [33] André Diatta, Younes Achaoui, Stéphane Brûlé, Stefan Enoch, Sébastien Guenneau, Control of Rayleigh-like waves in thick plate Willis
- metamaterials, AIP Adv. 6 (12) (2016) 121707, http://dx.doi.org/10.1063/1.4972280.
 [34] René Pernas-Salomón, Gal Shmuel, Dynamic homogenization of composite and locally resonant flexural systems, J. Mech. Phys. Solids 119 (2018) 43–59, http://dx.doi.org/10.1016/j.jmps.2018.06.011, http://www.sciencedirect.com/science/article/pii/S0022509618302503.
- [35] Alan Muhafra, Majd Kosta, Daniel Torrent, René Pernas-Salomón, Gal Shmuel, Homogenization of piezoelectric planar Willis materials undergoing antiplane shear, 2021, under revision for Wave Motion Special Issue entitled "Willis Materials". https://engrxiv.org/aswmt/.
- [36] Andrea Alù, First-principles homogenization theory for periodic metamaterials, Phys. Rev. B 84 (2011) 075153, http://dx.doi.org/10.1103/ PhysRevB.84.075153.
- [37] Andrea Alù, Restoring the physical meaning of metamaterial constitutive parameters, Phys. Rev. B 83 (2011) 081102, http://dx.doi.org/10.1103/ PhysRevB.83.081102.
- [38] René Pernas-Salomón, Gal Shmuel, Symmetry breaking creates electro-momentum coupling in piezoelectric metamaterials, J. Mech. Phys. Solids 134 (2020) 103770, http://dx.doi.org/10.1016/j.jmps.2019.103770, http://www.sciencedirect.com/science/article/pii/S0022509619306386.
- [39] J.R. Willis, Dynamics of composites, in: P. Suquet (Ed.), Continuum Micromechanics, in: International Centre for Mechanical Sciences (Courses and Lectures), 377, Springer, Vienna, 1997, pp. 265–290, http://dx.doi.org/10.1007/978-3-7091-2662-2_5.
- [40] Graeme W. Milton, New metamaterials with macroscopic behavior outside that of continuum elastodynamics, New J. Phys. 9 (10) (2007) http://dx.doi.org/10.1088/1367-2630/9/10/359, 359-359.
- [41] Graeme W. Milton, A unifying perspective on linear continuum equations prevalent in physics. Part II: Canonical forms for time-harmonic equations, 2020, ArXiv:2006.02433.
- [42] Sukmo Koo, Choonlae Cho, Jun-ho Jeong, Namkyoo Park, Acoustic omni meta-atom for decoupled access to all octants of a wave parameter space, Nature Commun. 7 (2016) 13012 EP -. https://doi.org/10.1038/ncomms13012.
- [43] Yan Kei Chiang, Sebastian Oberst, Anton Melnikov, Li Quan, Steffen Marburg, Andrea Alù, David A. Powell, Reconfigurable acoustic metagrating for high-efficiency anomalous reflection, Phys. Rev. Appl. 13 (2020) 064067, http://dx.doi.org/10.1103/PhysRevApplied.13.064067.
- [44] Yangyang Chen, Xiaopeng Li, Gengkai Hu, Michael R. Haberman, Guoliang Huang, An active mechanical Willis meta-layer with asymmetric polarizabilities, Nature Commun. 11 (1) (2020) 3681, http://dx.doi.org/10.1038/s41467-020-17529-2.
- [45] D.R. Smith, S. Schultz, P. Markoš, C.M. Soukoulis, Determination of effective permittivity and permeability of metamaterials from reflection and transmission coefficients, Phys. Rev. B 65 (2002) 195104, http://dx.doi.org/10.1103/PhysRevB.65.195104.
- [46] S. O'Brien, J.B. Pendry, Magnetic activity at infrared frequencies in structured metallic photonic crystals, J. Phys.: Condens. Matter 14 (25) (2002) 6383–6394, http://dx.doi.org/10.1088/0953-8984/14/25/307.
- [47] Vladimir Fokin, Muralidhar Ambati, Cheng Sun, Xiang Zhang, Method for retrieving effective properties of locally resonant acoustic metamaterials, Phys. Rev. B 76 (14) (2007) 144302, http://dx.doi.org/10.1103/PhysRevB.76.144302.
- [48] C.R. Simovski, On electromagnetic characterization and homogenization of nanostructured metamaterials, J. Opt. 13 (1) (2010) 013001, http://dx.doi.org/10.1088/2040-8978/13/1/013001.
- [49] René Pernas-Salomón, Gal Shmuel, Fundamental principles for generalized willis metamaterials, Phys. Rev. Appl. 14 (2020) 064005, http://dx.doi.org/10.1103/PhysRevApplied.14.064005.
- [50] B.A. Auld, Acoustic Fields and Waves in Solids, in: A Wiley-Interscience publication, Wiley, 1973, https://books.google.co.il/books?id=_2MWAwAAQBAJ.
- [51] S.J. Rupitsch, Piezoelectric Sensors and Actuators: Fundamentals and Applications, in: Topics in Mining, Metallurgy and Materials Engineering, Springer Berlin Heidelberg, 2018, https://books.google.co.il/books?id=2JdmDwAAQBAJ.
- [52] J.R. Willis, Mechanics of composites, 2002.
- [53] Michael B. Muhlestein, Benjamin M. Goldsberry, Andrew N. Norris, Michael R. Haberman, Acoustic scattering from a fluid cylinder with Willis constitutive properties, Proc. R. Soc. Lond. Ser. A Math. Phys. Eng. Sci. 474 (2220) (2018) 20180571.

- [54] A.A. Kutsenko, A.L. Shuvalov, O. Poncelet, A.N. Darinskii, Tunable effective constants of the one-dimensional piezoelectric phononic crystal with internal connected electrodes, J. Acoust. Soc. Am. 137 (2) (2015) 606–616, http://dx.doi.org/10.1121/1.4906162.
- [55] Shixu Meng, Bojan B. Guzina, On the dynamic homogenization of periodic media: Willis' approach versus two-scale paradigm, Proc. R. Soc. London A Math. Phys. Eng. Sci. 474 (2213) (2018) http://dx.doi.org/10.1098/rspa.2017.0638.
- [56] Xiaoshi Su, Andrew N. Norris, Retrieval method for the bianisotropic polarizability tensor of Willis acoustic scatterers, Phys. Rev. B 98 (2018) 174305, http://dx.doi.org/10.1103/PhysRevB.98.174305.
- [57] R. Pérez-Álvarez, F. García-Moliner, Transfer Matrix, Green Function and Related Techniques: Tools for the Study of Multilayer Heterostructures, Universitat Jaume I. Castellón de la Plana. Spain. 2004.
- [58] R.A. Horn, C.R. Johnson, Topics in Matrix Analysis, Cambridge University Press, Cambridge, 1991.
- [59] A.L. Shuvalov, A.A. Kutsenko, A.N. Norris, Divergence of logarithm of a unimodular monodromy matrix near the edges of the Brillouin zone, Wave Motion 47 (6) (2010) 370–382, http://dx.doi.org/10.1016/j.wavemoti.2009.12.005, http://www.sciencedirect.com/science/article/pii/S016521250900122X
- [60] M.C. Pease III, Methods of Matrix Algebra, Chap. VII, Sec. 4., Academic Press, New York, 1965, pp. 177-179.
- [61] Rémi Cornaggia, Bojan B. Guzina, Second-order homogenization of boundary and transmission conditions for one-dimensional waves in periodic media, Int. J. Solids Struct. 188–189 (2020) 88–102, http://dx.doi.org/10.1016/j.ijsolstr.2019.09.009, https://www.sciencedirect.com/ science/article/pii/S0020768319304202.